NAVAL POSTGRADUATE SCHOOL

MONTEREY, CALIFORNIA

THESIS

COMPUTATIONAL ANALYSIS OF FLOW THROUGH A TRANSONIC COMPRESSOR ROTOR

by

Nikolaus J. Bochette

September 2005

Thesis Advisor:	Garth Hobson
Second Reader:	Raymond Shreeve

Approved for public release; distribution is unlimited

THIS PAGE INTENTIONALLY LEFT BLANK

REPORT DOCUMENTATION PAGE			*Form Approved OMB No. 0704-0188*
Public reporting burden for this collection of information is estimated to average 1 hour per response, including the time for reviewing instruction, searching existing data sources, gathering and maintaining the data needed, and completing and reviewing the collection of information. Send comments regarding this burden estimate or any other aspect of this collection of information, including suggestions for reducing this burden, to Washington headquarters Services, Directorate for Information Operations and Reports, 1215 Jefferson Davis Highway, Suite 1204, Arlington, VA 22202-4302, and to the Office of Management and Budget, Paperwork Reduction Project (0704-0188) Washington DC 20503.			
1. AGENCY USE ONLY *(Leave blank)*	**2. REPORT DATE** September 2005	**3. REPORT TYPE AND DATES COVERED** Master's Thesis	
4. TITLE AND SUBTITLE: Computational Analysis of Flow Through a Transonic Compressor Rotor			**5. FUNDING NUMBERS**
6. AUTHOR(S) Nikolaus J. Bochette			
7. PERFORMING ORGANIZATION NAME(S) AND ADDRESS(ES) Naval Postgraduate School Monterey, CA 93943-5000			**8. PERFORMING ORGANIZATION REPORT NUMBER**
9. SPONSORING /MONITORING AGENCY NAME(S) AND ADDRESS(ES) N/A			**10. SPONSORING/MONITORING AGENCY REPORT NUMBER**
11. SUPPLEMENTARY NOTES The views expressed in this thesis are those of the author and do not reflect the official policy or position of the Department of Defense or the U.S. Government.			
12a. DISTRIBUTION / AVAILABILITY STATEMENT Approved for public release; distribution is unlimited.			**12b. DISTRIBUTION CODE**

13. ABSTRACT (maximum 200 words)

As the United States Navy prepares to field a single engine jet, the F-35C Joint Strike Fighter, it is important that the causes of the "pop-stall" occurrence be understood. This problem arises as the jet engine ingests steam just prior to being released from the catapult. In examining this problem two Computational Fluid Dynamic (CFD) codes have been used by the Naval Postgraduate School to predict the performance of a transonic compressor rotor that is being tested with steam ingestion. Both codes, developed by NASA, provide a baseline that experimental results and new CFD codes can be compared with. Ansys Inc., a commercial Computer Aided Design (CAD) software company, has developed a new code that allows modeling of two phase flow. ICEM-CFD and CFX-5, both Anys Inc. programs that can model turbomachinery blade passages similar to that used by the NASA codes, were used in the present study. Comparisons were made with the experimental data and the predictions made by NASA codes as part of the initial modeling of the transonic compressor rotor flow field.

14. SUBJECT TERMS Compressor, Transonic, Steam Ingestion, Computational Fluid Dynamics (CFD), Turbo-machinery, Pop-stall, Rotor, Shock Waves	**15. NUMBER OF PAGES** 71
	16. PRICE CODE

17. SECURITY CLASSIFICATION OF REPORT	**18. SECURITY CLASSIFICATION OF THIS PAGE**	**19. SECURITY CLASSIFICATION OF ABSTRACT**	**20. LIMITATION OF ABSTRACT**
Unclassified	Unclassified	Unclassified	UL

NSN 7540-01-280-5500 Standard Form 298 (Rev. 2-89)
Prescribed by ANSI Std. 239-18

THIS PAGE INTENTIONALLY LEFT BLANK

Approved for public release; distribution is unlimited

COMPUTATIONAL ANALYSIS OF FLOW THROUGH A TRANSONIC COMPRESSOR ROTOR

Nikolaus J. Bochette
Ensign, United States Navy
B.S., United States Naval Academy, 2004

Submitted in partial fulfillment of the
requirements for the degree of

MASTER OF SCIENCE IN MECHANICAL ENGINEERING

from the

NAVAL POSTGRADUATE SCHOOL
September 2005

Author: Nikolaus J. Bochette

Approved by: Dr. Garth Hobson
Thesis Advisor

Dr. Raymond Shreeve
Second Reader

Dr. Anthony Healey
Chairman, Department of Mechanical and Astronautical Engineering

THIS PAGE INTENTIONALLY LEFT BLANK

ABSTRACT

As the United States Navy prepares to field a single engine jet, the F-35C Joint Strike Fighter, it is important that the causes of the "pop-stall" occurrence be understood. This problem arises as the jet engine ingests steam just prior to being released from the catapult. In examining this problem two Computational Fluid Dynamic (CFD) codes have been used by the Naval Postgraduate School to predict the performance of a transonic compressor rotor that is being tested with steam ingestion. Both codes, developed by NASA, provide a baseline that experimental results and new CFD codes can be compared with. Ansys Inc., a commercial Computer Aided Design (CAD) software company, has developed a new code that allows modeling of two phase flow. ICEM-CFD and CFX-5, both Anys Inc. programs that can model turbomachinery blade passages similar to that used by the NASA codes, were used in the present study. Comparisons were made with the experimental data and the predictions made by NASA codes as part of the initial modeling of the transonic compressor rotor flow field.

THIS PAGE INTENTIONALLY LEFT BLANK

TABLE OF CONTENTS

THIS PAGE INTENTIONALLY LEFT BLANK

LIST OF FIGURES

THIS PAGE INTENTIONALLY LEFT BLANK

LIST OF TABLES

THIS PAGE INTENTIONALLY LEFT BLANK

ACKNOWLEDGMENTS

I would like to thank both Professor Hobson and Professor Shreeve for allowing me the opportunity to work with them. They are a wealth of knowledge and were eager to pass it on to me, even if it had to be explained more than once.

I would also like to thank Rick Still and John Gibson. Always quick with a joke and able to fix anything I broke. Without their vast knowledge of computer repair I might still be running simulations.

The TPL is a wonderful and rewarding place to work. It was an opportunity that I am grateful for having participated in.

THIS PAGE INTENTIONALLY LEFT BLANK

I. INTRODUCTION

As the United States Navy transitions to the F-35C Joint Strike Fighter (JSF) it is paramount that the "pop-stall" phenomenon be resolved. Experiments conducted at Lakehurst Naval Air Engineering Station, using current aircraft, show that just prior to release on catapult assisted launches various amounts of steam are being ingested into the engines. This steam ingestion can lead to a stall and surge of the engine which causes a temporary loss of power. The experiment at Lakehurst was conducted with an F-18 Hornet which is a dual engine aircraft utilizing General Electric (GE) engines. The F-35C JSF is a single engine aircraft that uses the Pratt & Whitney F-135 engine. If the F-35C JSF's only engine were to stall at launch the results could be catastrophic. (Donelson, 2003)

Concentration has now been focused on the "Pop-Stall" problem. The Turbopropulsion Laboratory (TPL) at the Naval Postgraduate School (NPS) is investigating fundamental aspects of the issue using its Transonic Compressor Rig (TCR). In 2000 the TCR was rebuilt, after an initial failure of the rotor spinner, and re-instrumented by Joseph O'Brien. (O'Brien, 2000)

Nelson Sanger designed the present transonic fan stage. He designed the stage specifically for the Naval Postgraduate School to use in their Transonic Compressor Rig (TPR). The design relied heavily on Computational Fluid Dynamic (CFD) techniques while minimizing conventional empirical design methods. For the design Sanger used the Denton Code, which employed an Euler Solver. (Sanger, 1996 and 1999) Figure 2 shows a picture of the rotor as tested by Gannon. (Gannon et. al., 2005)

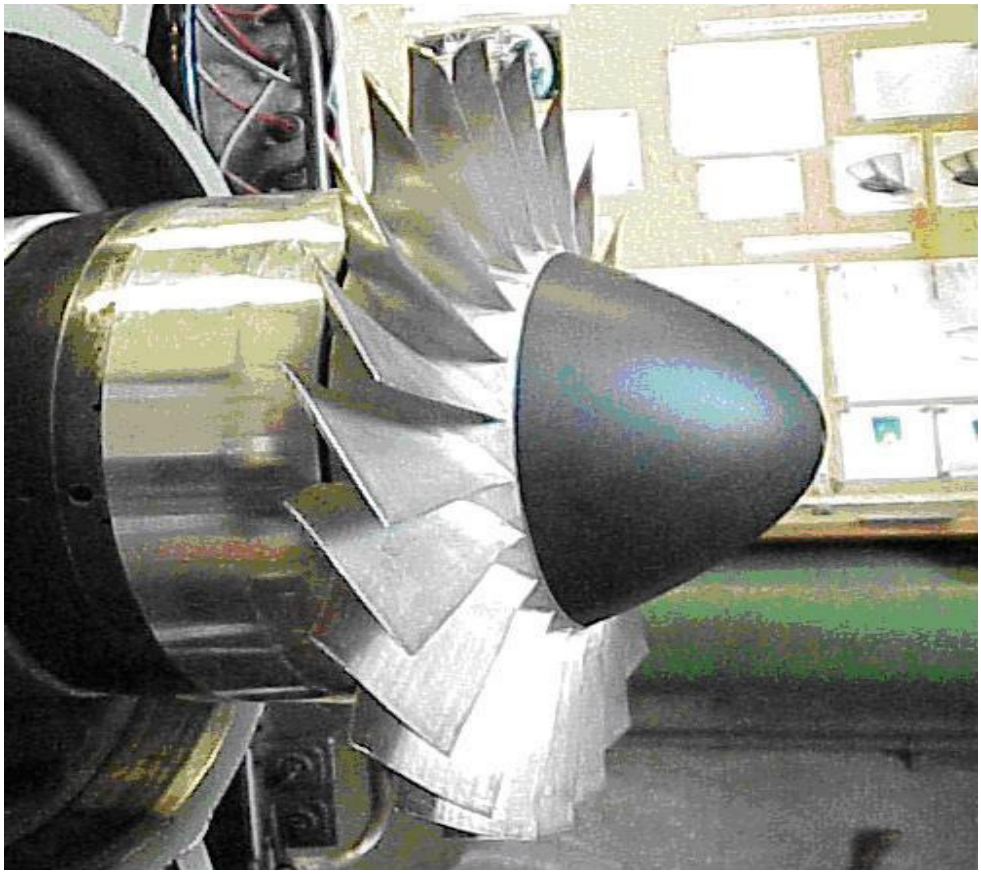

Figure 1. Sanger Rotor On Transonic Compressor Rig

Since the rebuild in 2000, measurements have included performance measurements from fixed probes and, more recently, survey measurements to gain an understanding of the airflow. A three-hole probe was initially used to determine pressure and Mach number profiles at different stations along the case wall. (Villescas, 2005) Based upon recommendations from that study a five-hole probe was used to take measurements in the same fashion. (Brunner, 2005) CFD studies have been conducted in conjunction with the experimental program to predict the stage performance. (Gannon et. al. 2004) (Hobson et. al. 2004)

More recently, two CFD codes developed by NASA have been used to model the Sanger rotor-only configuration and provide baseline results with which to compare future codes. (Gannon et. al., 2005) The current study used a commercial code, developed by Ansys Inc., which was capable of modeling two phase flow through a transonic compressor rotor. The “turbo-mode” in ICEM-CFD was used to create a mesh

that modeled a single blade passage. The model was loaded into CFX-5 and simulations were run at 90% and 100% speed. The results from these simulations are compared to the baseline results provided by the NASA codes.

THIS PAGE INTENTIONALLY LEFT BLANK

II. PREVIOUS WORK

A. SWIFT CODE

The SWIFT code was developed by Dr. R.V. Chima at the NASA Lewis Research Center in Cleveland, OH. (Chima, 1998) It solved the thin-layer Navier-Stokes equations with the Baldwin-Lomax or k-ω turbulence models using an explicit Runge-Kutta method. The SWIFT code used structured C-grids around blade profiles. After running initial simulations with this mesh it was determined that an inlet grid was needed to resolve the upstream shock system relative to the rotor blade. Figure 3 shows the Total-to-Total Pressure Ratio vs. Mass Flow Rate results for 100% speed from the original mesh (magenta) and revised mesh (green) as well as the data obtained from experiments. From the graph it is obvious that having this inlet grid impacted the accuracy of the results. The inlet grid lowered the speed curve so that it more closely matched the experimental data. (Gannon et. al., 2005)

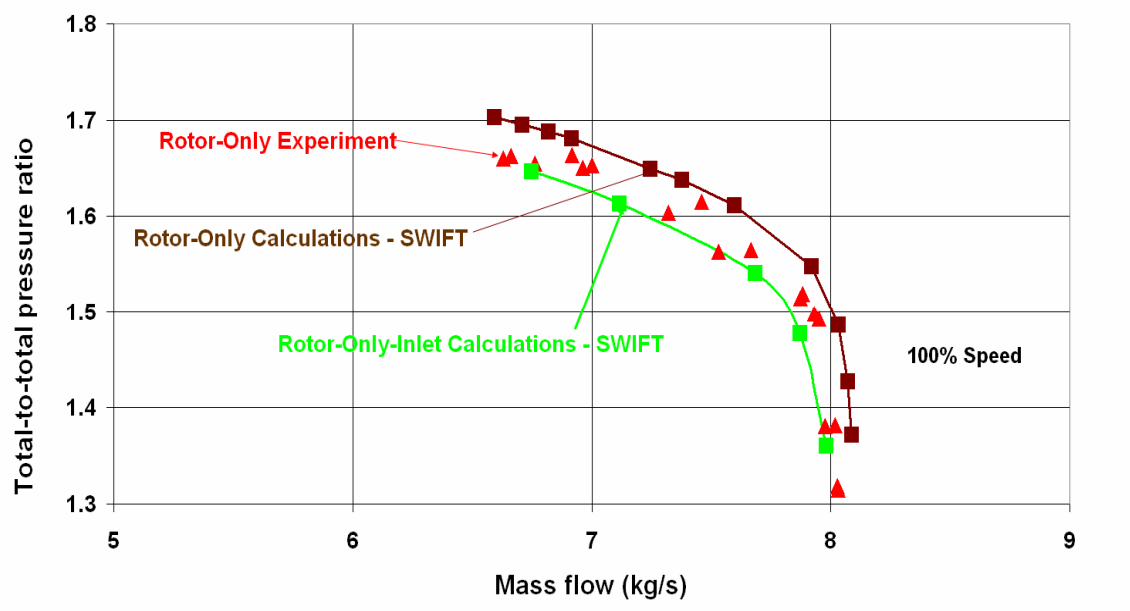

Figure 2. SWIFT Code: Total-to-Total Pressure Ratio vs. Mass Flow Rate

Figure 4 shows the Isentropic Efficiency vs. Mass Flow Rate for 100% speed, once again, for the SWIFT Code. Notice that before the inlet grid was in place that the

code over predicted the efficiency by 6%. After the inlet grid was installed the efficiency was still over predicted however, the percentage dropped by a factor of two from 6% to 3%. This data shows the importance that the inlet grid had in predicting the performance. The resulting grid size for the inlet and the rotor blade was 329,572 grid points.

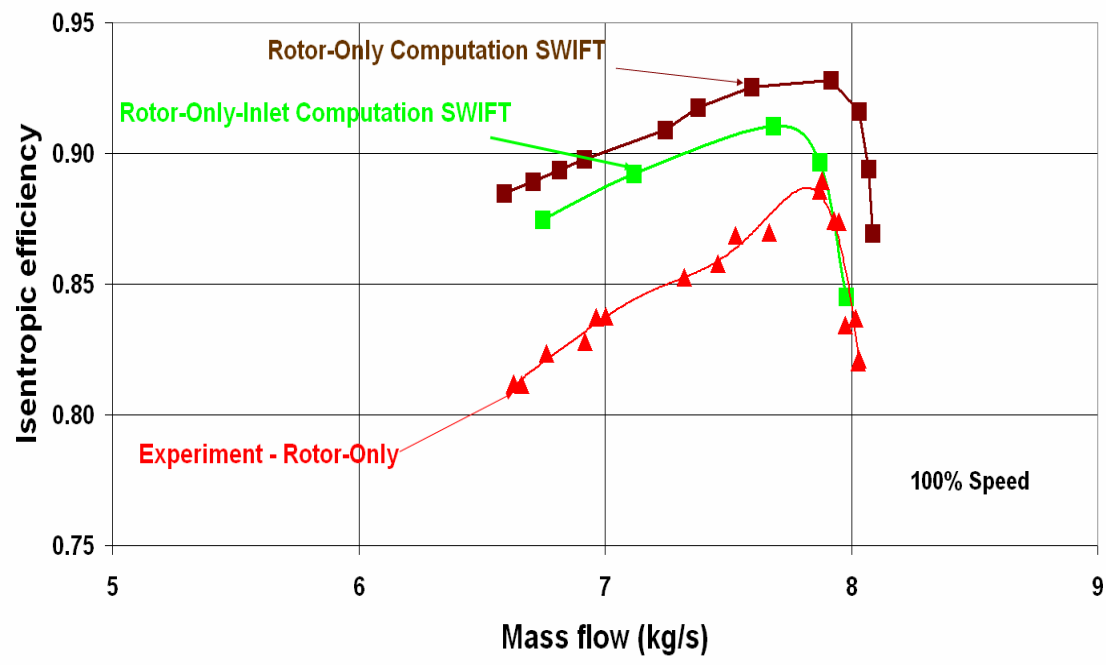

Figure 3. SWIFT Code: Isentropic Efficiency vs. Mass Flow Rate

B. TURBO CODE

The TURBO Code was developed by Dr. Jenping Chen of Mississippi State University and Dr. Michael Hathaway at the NASA Glenn Research Center in Cleveland, OH. It used an implicit algorithm to solve the full Navier-Stokes equations and it utilized a structured "H"-grid within the blade passage. It also allowed for parallelization and multi-block domain decomposition for full blade row simulations. This would allow the tracking of stall cells that develop in the compressor. Figure 5 displays the comparison of the Total-to-Total Pressure Ratio vs. Mass Flow Rate between the TURBO Code, SWIFT Code, and experimental data. Once again, it is for 100% speed. The TURBO Code predicted the pressure ratio between the two SWIFT Code predictions. Figure 6 displays the comparison of the Isentropic Efficiency vs. Mass Flow Rate between the TURBO Code, SWIFT Code, and experimental data at 100% speed. Once more, the TURBO Code predicted values that were between the two SWIFT Code predictions. The

difference between the SWIFT Code with the inlet and the TURBO Code increased toward the choke position. At lower mass flow rates the TURBO Code and the SWIFT Code with an inlet grid are in good agreement. The total grid size for the TURBO code was 362,600 grid points. This was a very fine mesh which was formed to produce accurate results. (Hobson, 2005)

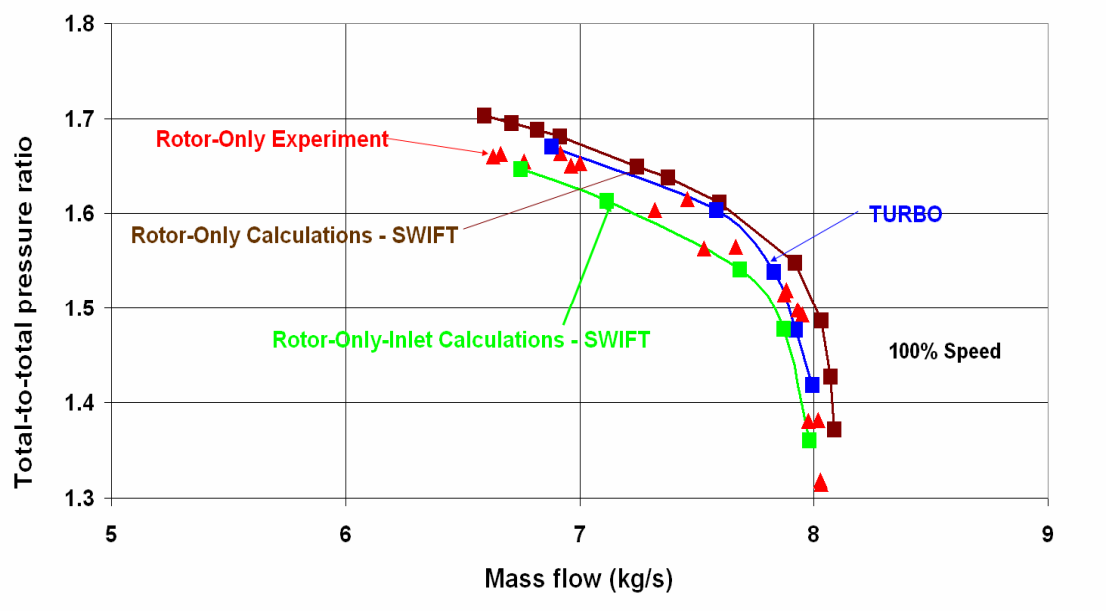

Figure 4. TURBO Code: Total-to-Total Pressure Ratio vs. Mass Flow Rate

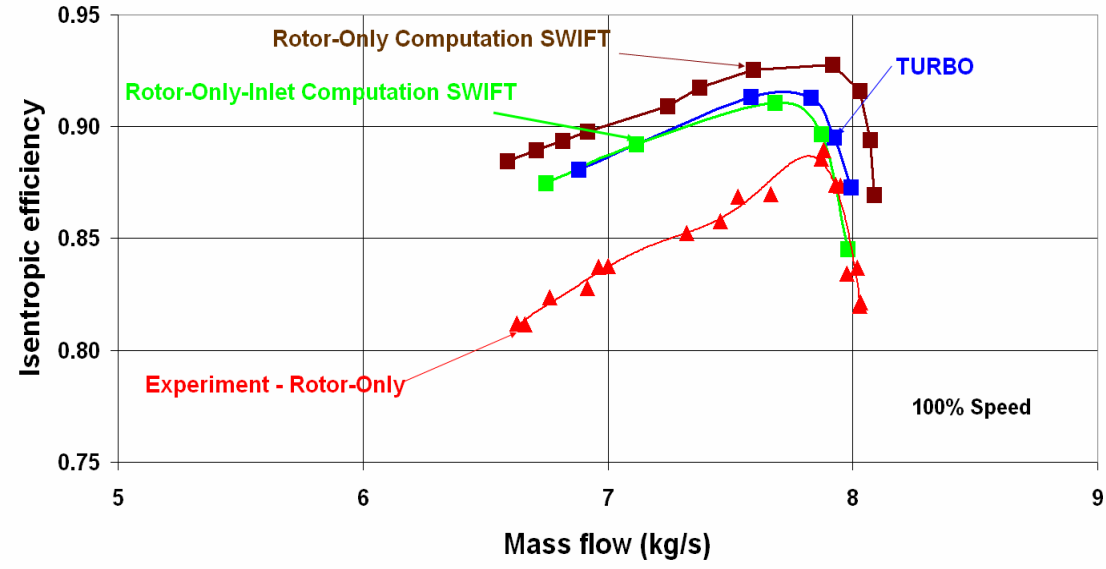

Figure 5. TURBO Code: Isentropic Efficiency vs. Mass Flow Rate

THIS PAGE INTENTIONALLY LEFT BLANK

III. PROCEDURES

A. ICEM-CFD

ICEM-CFD was a Computer Aided Design (CAD) program that was compatible with CFX-5. After creating a CAD model it allowed the user to generate one of three types of meshes: structured, unstructured, or hybrid. To begin the process the user would import geometry information. Assuming that the only information available was a set of (x,y,z) coordinates the user would next have to generate lines through those coordinates to develop the shape of the object being modeled. Following the line generation, surfaces were created from the lines to yield a solid 3-dimensional object. After the object was modeled, a unique ability within ICEM-CFD was activated to turn on the "turbo" mode. Under the Mesh tab there are thirteen functions to choose from, the first of which was *Set Global Mesh Size*. Clicking on this button activated a side menu with a scroll bar. The user scrolled to the bottom of the side menu and turned on the *Define periodicity*. After turning the button on, one had to ensure that the *Type* was set to *Rotational Periodic* and that the *Axis* option was set to the axis of rotation and that the *Angle* option was set to the angle that separated the blades. For the Sanger rotor this angle was sixteen and four-elevenths degrees. Clicking on the *Apply* button activated the "turbo" mode. By defining the object as rotationally periodic the software knew that the mesh it generated for one periodic face had to be the same for the other periodic face. Figures 7 and 8 illustrate the process just described. (Ansys, 2005) (Harwell, 2005)

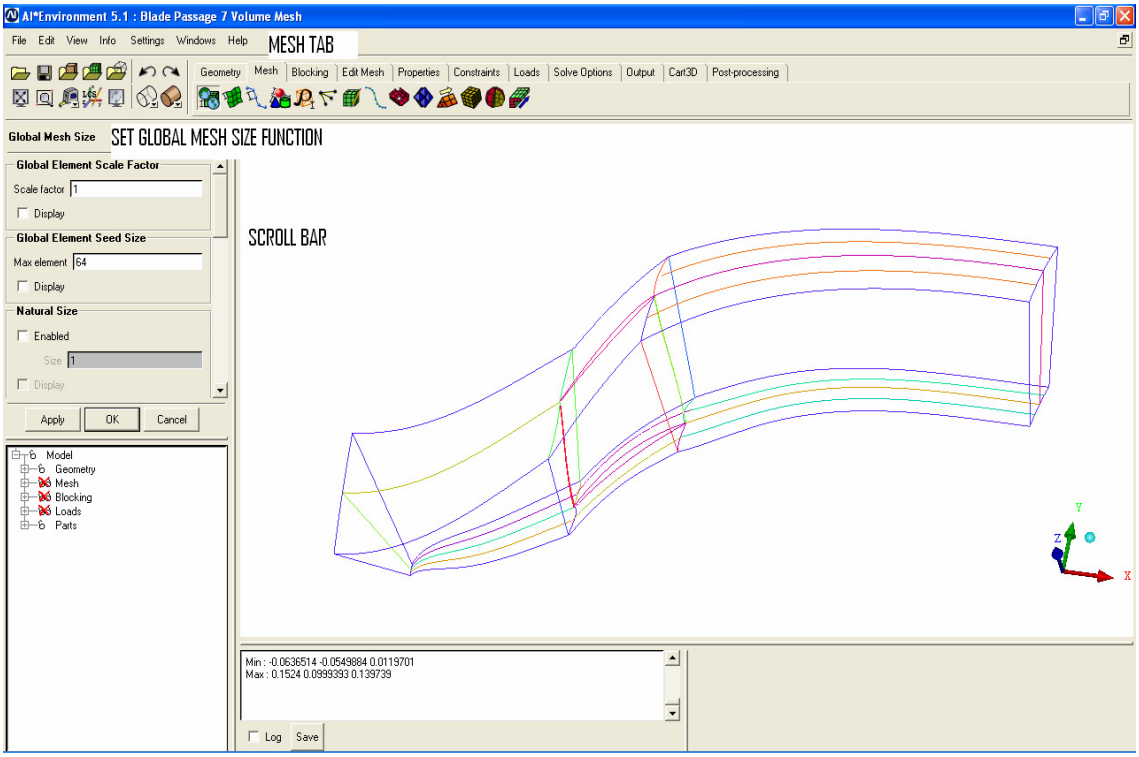

Figure 6. ICEM-CFD: Setting Turbo Mode

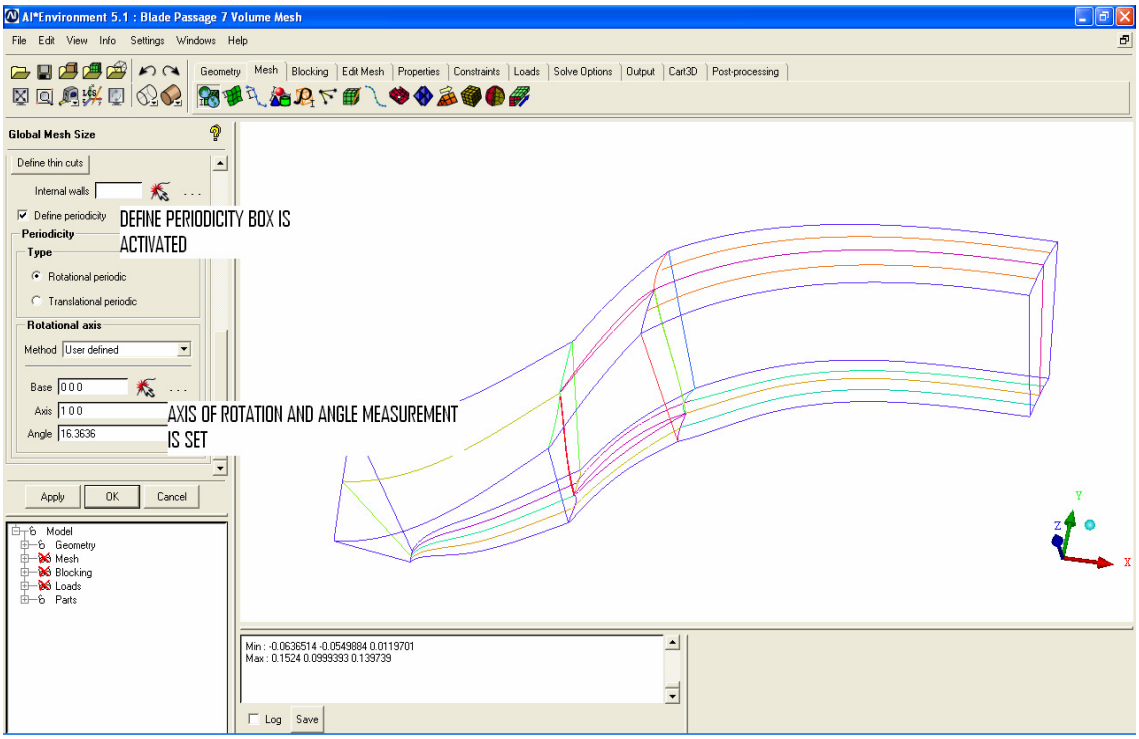

Figure 7. ICEM-CFD: Periodicity Of the CAD Drawing is Activated.

After an acceptable model was created, the user had to decide what type of mesh to use. In the present study, it was found that trying to create a structured or unstructured mesh with the complicated geometry of Blade Passage was not possible. Therefore, a hybrid mesh was created. Table 1 shows the number of elements on each surface of the passage as well as giving the total number of elements in the grid.

Part Name	Number of Elements
Blade	3,920
Hub	2,944
Shroud	2,944
Inlet	1,225
Outlet	1,225
Symmetry 1	2,695
Symmetry 2	2,695
Total Surfaces	14,704
Volume	148,195
Total Mesh Size	162,899

Table 1. ICEM-CFD: Number Of Elements Within the Mesh

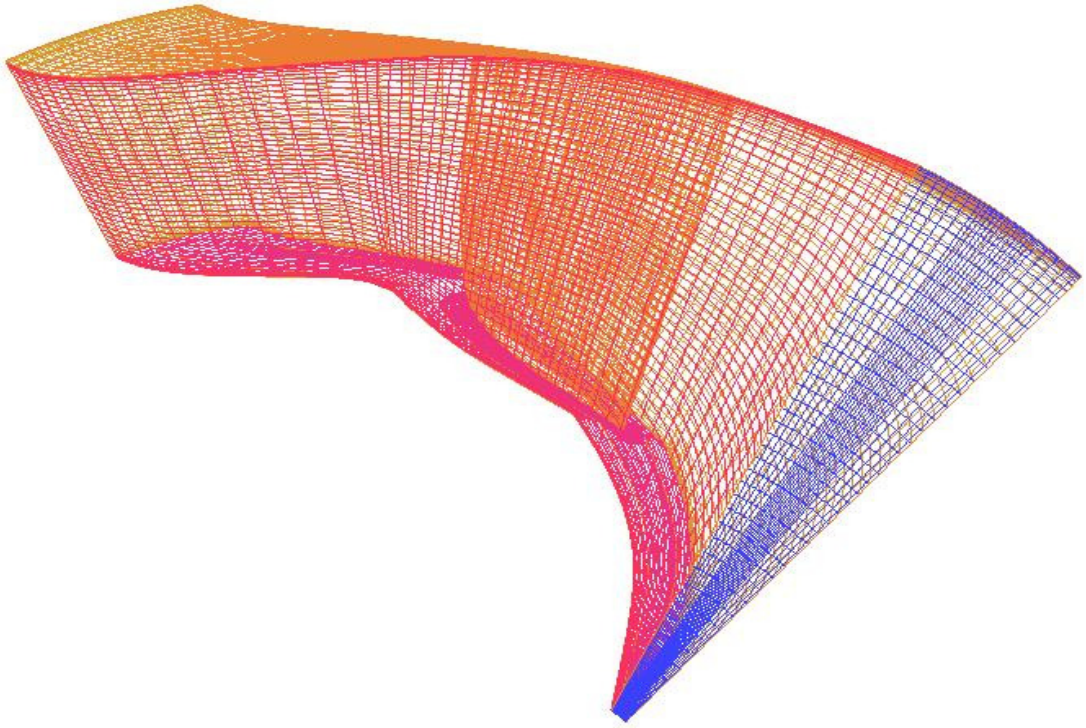

Figure 8. ICEM-CFD: Blade Passage Surface Mesh

It was important to notice that this grid had 162,899 elements, one-third the number of elements of the previous two codes. This had to be kept in mind when comparing results to the previous CFD studies. Such a coarse grid would only give reasonably accurate results. Figure 9 shows the surface grids that are outlined in Table 1. (Ansys, 2005) To create a working mesh, a hybrid grid was created. An "O"-grid was created around the blade with the node spacing growing exponentially from the blade. Next, an "H"-grid was developed through the passage with nodes clustered towards both the tip and hub. This allowed more elements to be placed near the hub and tip so that the boundary layers could be resolved around the blade and end-wall surfaces. The model was also created with a zero clearance tip gap, hence the blade scrapped against the casing in the present simulation.

B. CFX-5

CFX-5 had three modules within it: CFX-Pre, CFX-Solver, and CFX-Post. Each module had specific attributes that made it desirable for turbomachinery flows.

The most important aspect of CFX-Pre was that it also had a "turbo" mode. When beginning a new simulation one option available to the user was "turbo". Highlighting this option specified that turbomachinery flows were being modeled. CFX-Pre was capable of reading multiple grids from multiple sources to simulate multi-blade-rows. Not only could it read multiple grids, but it also had a complex model library for complex flow physics specification. (Ansys, 2005) This allowed the user to model multi-phase flow through turbomachinery. (Brunner, 2005)

The CFX-Solver used a coupled algebraic multi-grid solver to solve the Navier-Stokes equations. It had first-order and second-order accurate advection schemes, as well as parallelization for automatic domain decomposition. (Ansys, 2005) This would allow an entire blade row to be modeled and solved simultaneously vice a single passage. However, that is beyond the scope of the present study.

CFX-Post also had a unique "turbo" mode for flow visualization. It allowed the user to view the meridional, blade-to-blade, and axial results. The user could take the results from a single passage and rotate them any number of times to produce an image,

as shown in Figure 10. The single blade passage was copied and rotated an additional ten times to produce a total of eleven blades (half of the Sanger rotor). This figure will be described in more detail at a later section. CFX-Post also allowed both the relative and absolute frames to be viewed and manipulated. CFX-Post will be discussed in the results section.

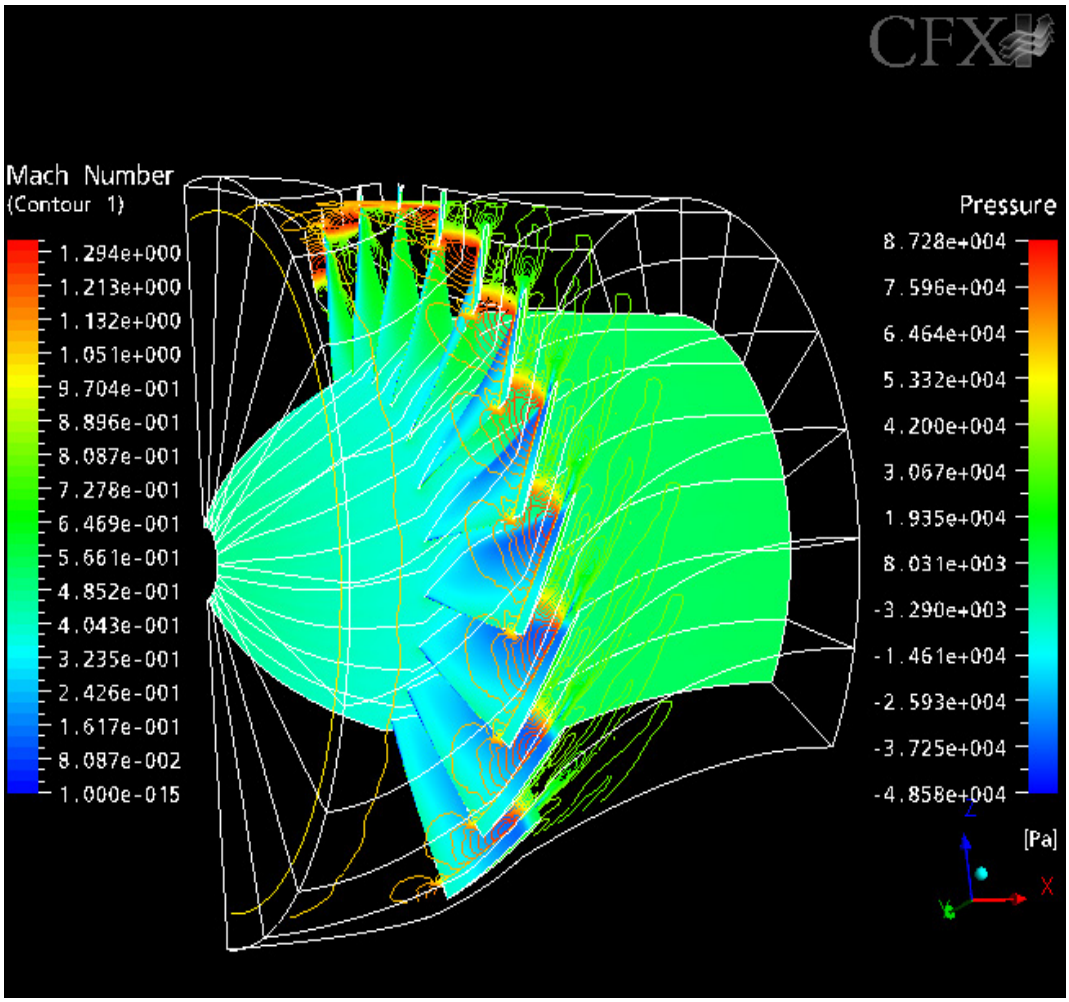

Figure 9. CFX-5: Blade Passage 7 With Pressure Along the Hub and Blade. The Contour Lines are the Mach Number.

1. CFX-Pre

To predict the performance of the model at 90% and 100% speed the model was initialized with air as an ideal gas. The *reference pressure* was set at 101 kPa. This meant that gauge pressures had to be used for setting the boundary conditions. This was

important because if the subsequent pressures were not gauge then the density of the air would be incorrectly calculated, which led to a mass flow rate that was incorrect. Since the Sanger rotor was being modeled, the *domain motion* was set to *rotating*. However, the inlet velocity had to be defined in the stationary frame. Therefore, it was necessary to change the frame type on the *initialization* tab to *stationary*. The inlet velocity for 90% speed was set at 80 meters per second for the "x" direction and 0 meters per second for the "y" and "z" direction. For 100% speed the "x" component was changed to 115 meters per second (to account for the higher mass flow). For 90% speed the angular velocity input was 2552.7 radians per second. For 100% speed the value was changed to 2836.3 radians per second. The last item needing to be defined was the axis of rotation.

Even though the domain motion was set to rotating, the static pressure was also defined in the stationary frame. To ensure that accurate results were obtained it was necessary to change the inlet and outlet *frame type* to *stationary*. This was done by editing the inlet and outlet boundary conditions. On the *basic settings* tab the *frame type* had to be changed from *rotating* to *stationary*. If this change was not made then an error message would result in the solver because not enough mass flow was being induced through the passage. Once the *frame type* was changed, the *static pressure* could be set. For the inlet it was always 0 kPa. This was due to the reference pressure being set at 101 kPa. The inlet condition was not changed, and to simulate throttling along a speed line, the outlet static pressure was increased. Table 2 shows the back pressures used to obtain the data for the speed curves. Appendix C contains the procedure to develop the blade passage.

Simulation Number	Speed	Exit Static Pressure (kPa)
1	90%	8
2	90%	10
3	90%	12
4	90%	14
5	90%	14.5
6	90%	14
7	90%	16
8	90%	18
9	90%	20
10	90%	22
11	90%	24
12	90%	26
13	100%	10
14	100%	12
15	100%	14
16	100%	16
17	100%	18
18	100%	20
19	100%	22
20	100%	24
21	100%	26

Table 2. CFX-5: Simulations Conducted at 90% and 100% Speeds.

2. CFX-Solver

Once the definition file from CFX-Pre was loaded into the CFX-Solver, two important options arose. The first was whether or not a previous results file was needed to initialize the values of the current run. This was useful if boundary conditions needed to be changed during a simulation. For example if the user began by defining an exit mass flow rate but needed to change that to an exit static pressure, then he/she would stop the run, go into CFX-Pre and change the condition. Next a new definition file was created and when the CFX-Solver module began, it loaded the results file from the previous run in the *initial values* field. The new run would begin where the old run finished. Figure 11 displays the residuals for a 100% speed simulation on the rotor passage. The back pressure for this simulation was 126 kPa (or 26 kPa in the Outlet condition)

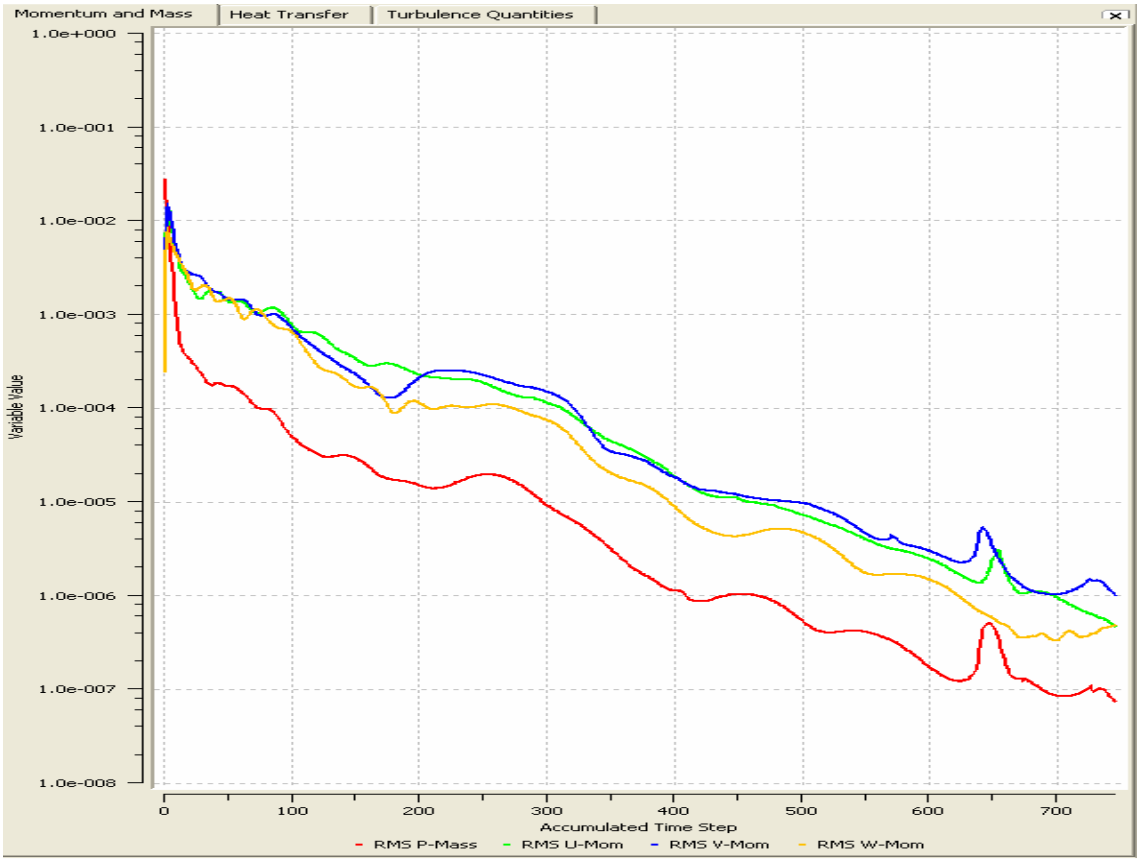

Figure 10. Residual Plot of U, V, and W Momentum and Pressure Mass for Simulation 21 From CFX-5.

The residual plot indicated that the x, y, and z momentum equation had converged due to the lines decreasing by four orders of magnitude. If the lines had converged through five orders of magnitude then the pressure would have converged as well. A timescale of 1E-5 was used, and the k and epsilon values were defaulted to 0.05 and 1 respectively.

The second option was the ability to use the parallelization of CFX-5. (Ansys, 2005) The user had the option to set up a serial run, a parallel run on the same computer, or a parallel run on a network. For full blade row simulations this becomes useful as the software will distribute the grid amongst the network based on the availability and processing power of the computers connected to the network. This option was not used in the present study.

IV. RESULTS AND DISCUSSION

A. 90% SPEED SIMULATION

Figures 12 and 13 show the results from CFX-5 plotted for comparison with previous data. Near stall, the CFX-5 results over predicted the pressure ratio. Near choke the CFX-5 results under predicted the mass flow rate by 3%. Close to stall the code over predicted the pressure ratio by 3%. However, at the flow rate giving peak efficiency experimentally the CFX-5 results were in agreement with experimental data. At flow rates below peak efficiency, the CFX-5 code over predicted the efficiency.

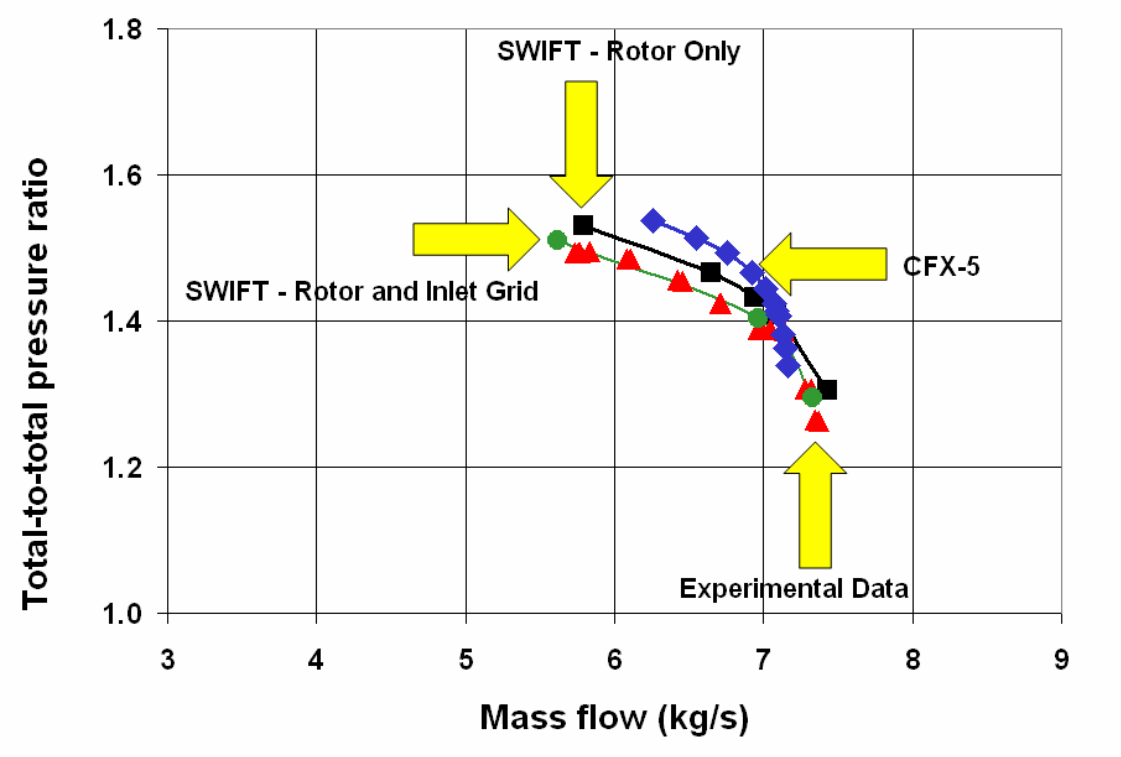

Figure 11. Total-to-Total Pressure Ratio vs. Mass Flow Rate for 90% speed

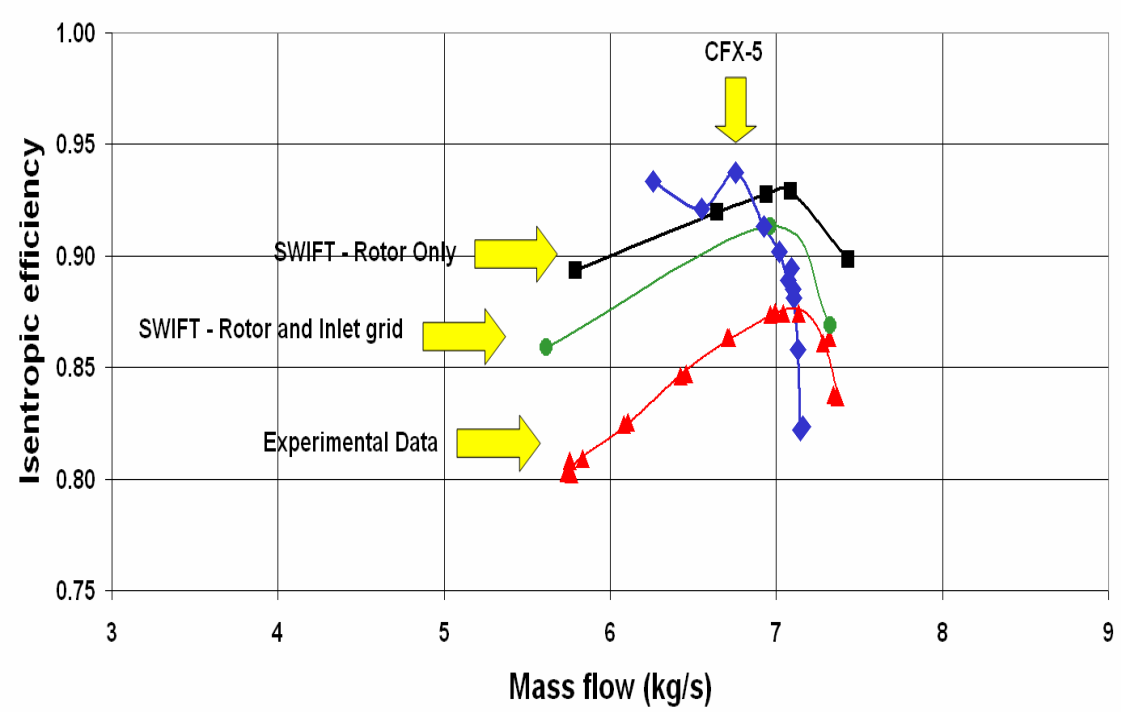

Figure 12. Isentropic Efficiency vs. Mass Flow Rate for 90% Speed

B. 100% SPEED SIMULATION

Figures 14 and 15 show the results from CFX-5 plotted in comparison with previous data. Near choke, the CFX-5 results under predicted the mass flow rate by 4%. The peak efficiency was not reached because the runs were not extended to include a back pressure that was sufficiently high.

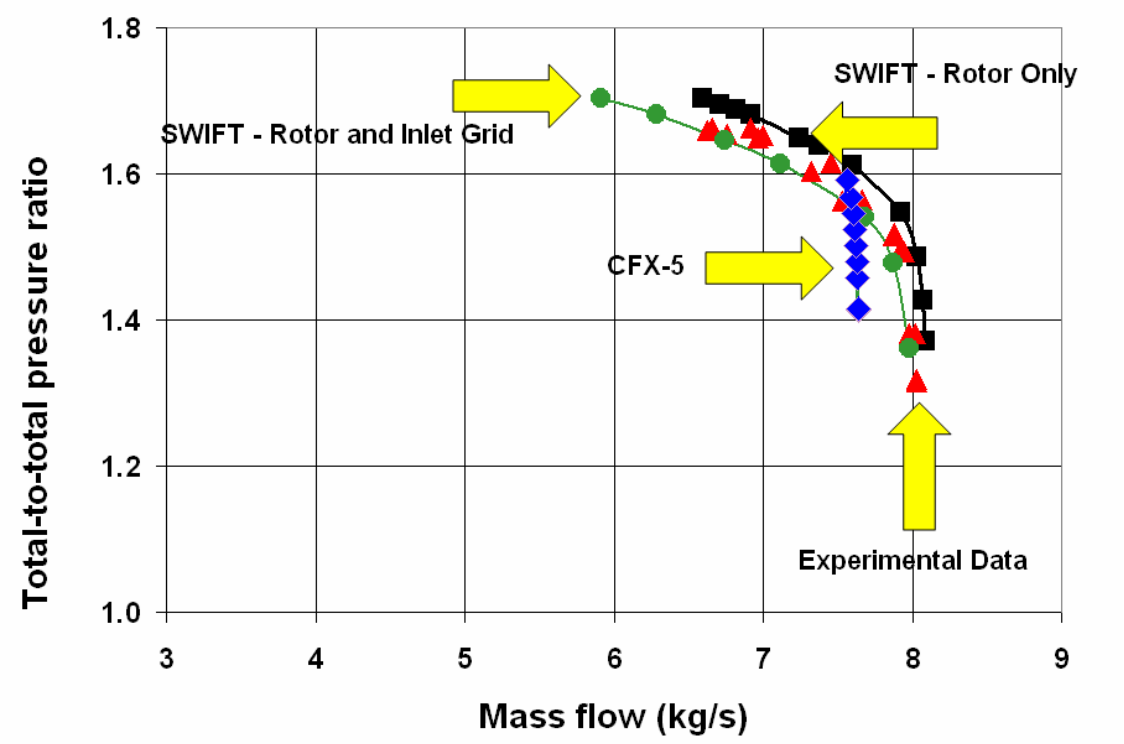

Figure 13. Total-to-Total Pressure Ratio vs. Mass Flow Rate for 100% Speed.

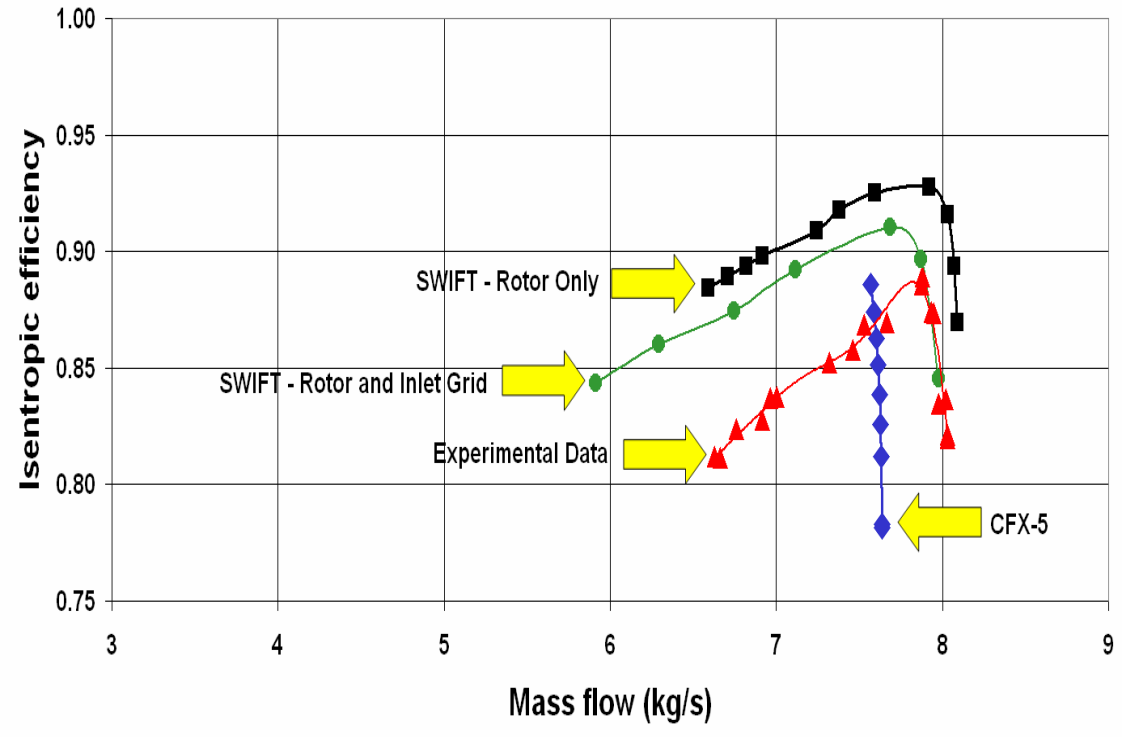

Figure 14. Isentropic Efficiency vs. Mass Flow Rate for 100% Speed

C. EXIT MACH NUMBER

Simulations were performed at 90% and 100% speeds. The Mach number distributions obtained are plotted in Figures 16 and 17. The plots show the exit Mach number vs. hub-to-tip ratio. The results are compared to results of probe measurements obtained by Villescas. (Villescas, 2005) The CFX-5 results were obtained with a back pressure of 112 kPa, corresponding to choke. Graphs of each simulation are found in Appendix A.

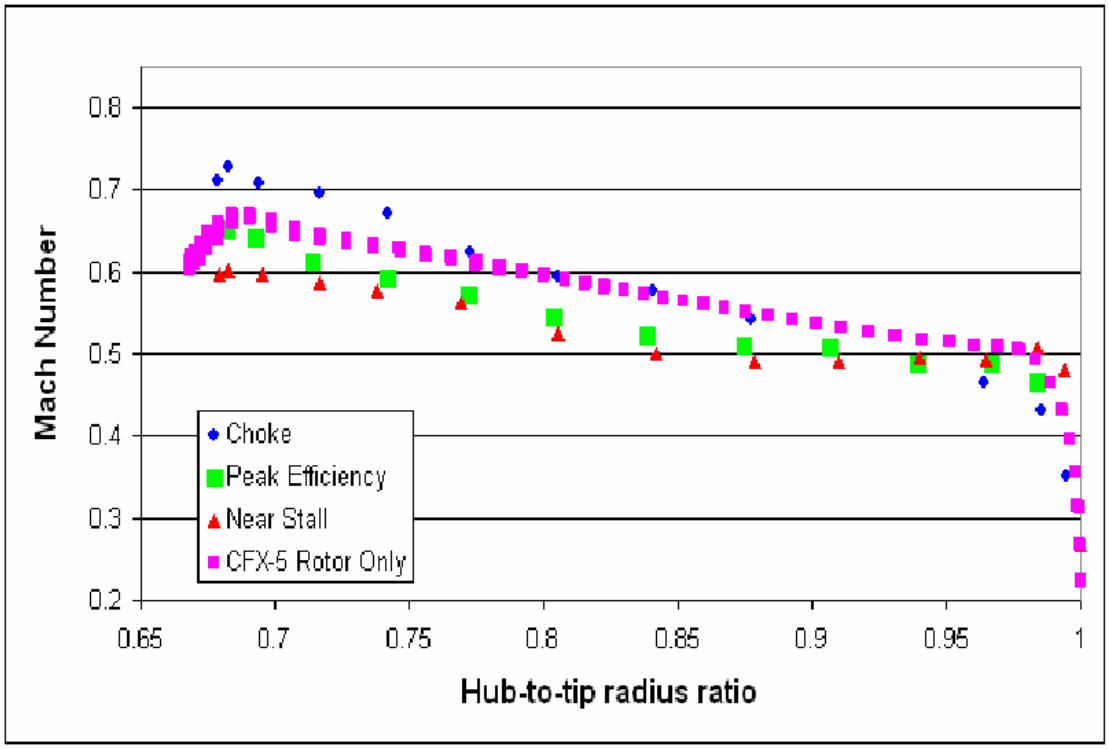

Figure 15. Exit Mach Number vs. Hub-to-Tip Radius Ratio for 90% Speed (CFX-5: Back Pressure = 112 kPa).

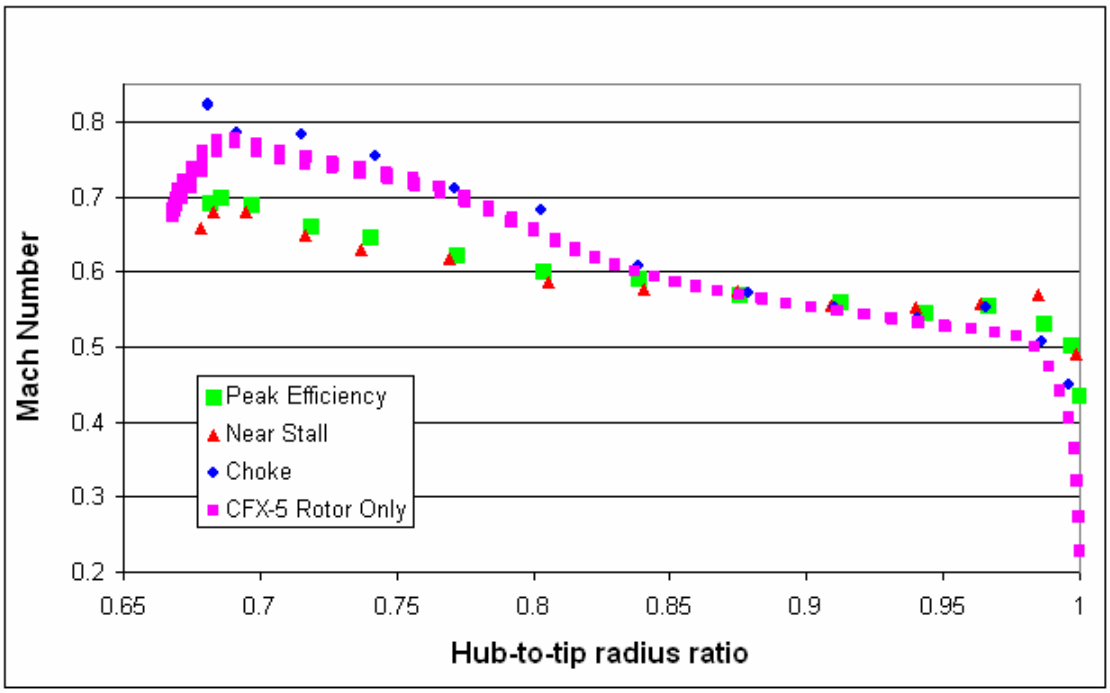

Figure 16. Exit Mach Number vs. Hub-to-Tip Radius Ratio for 100% Speed (CFX-5: Back Pressure = 112 kPa).

D. EXIT PRESSURE RATIO

The stagnation pressure ratio distributions obtained are plotted in Figures 18 and 19. The plots show the exit stagnation pressure ratio vs. hub-to-tip radius ratio. The results are compared to results of probe measurements obtained by Villescas. (Villescas, 2005) Graphs of each simulation are found in Appendix B. Again, the CFX-5 results were obtained with a back pressure of 112 kPa, corresponding to choke. The computed profiles are seen to be contained within the spread of the three experimental profiles. The level of the pressure rise is above that measured experimentally at choke, but corresponds to a lower than measured value of mass flow rate.

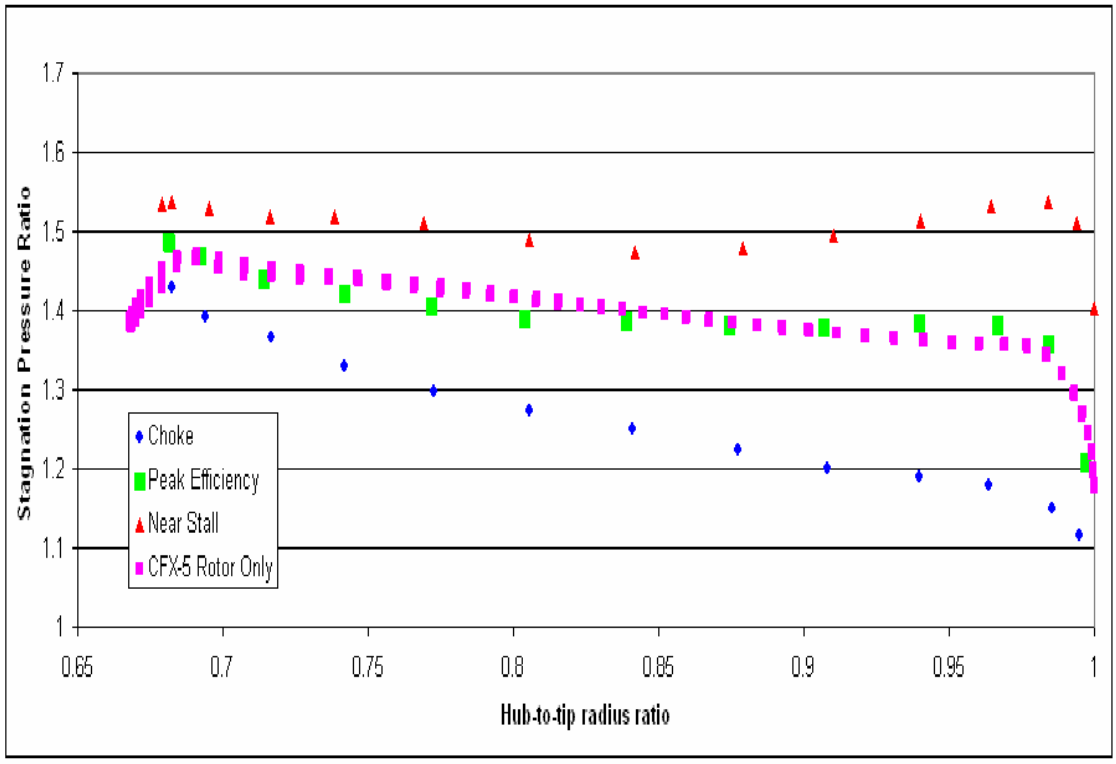

Figure 17. Stagnation Pressure Ratio vs. Hub-to-Tip Radius Ratio for 90% Speed (CFX-5: Back Pressure = 112 kPa).

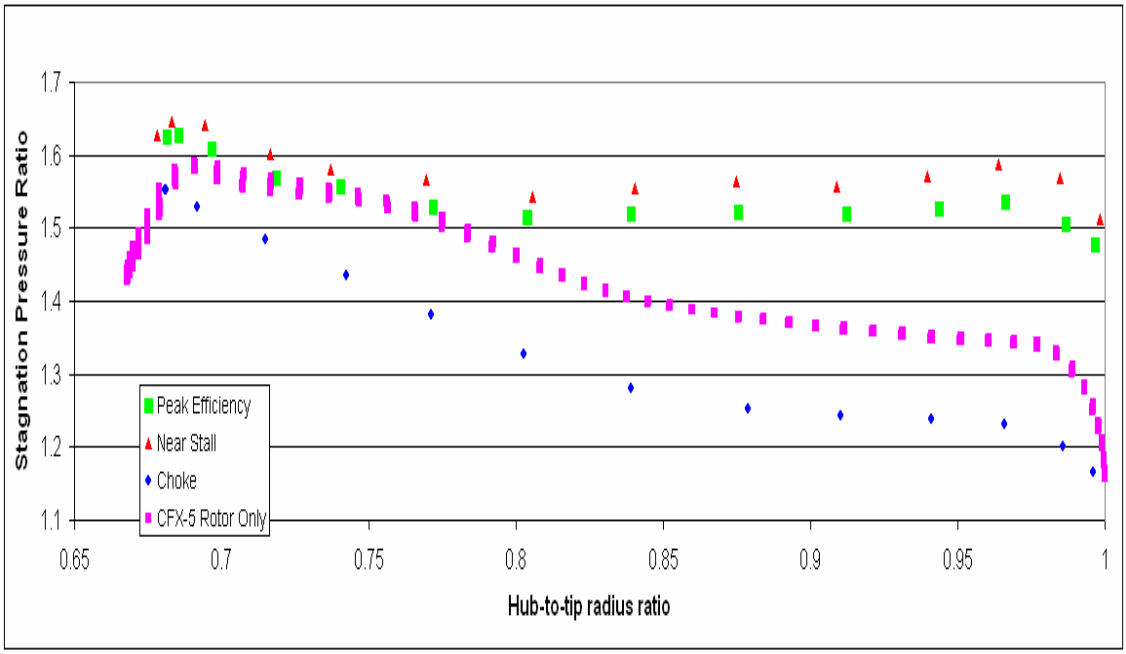

Figure 18. Stagnation Pressure Ratio vs. Hub-to-Tip Radius Ratio for 100% Speed (CFX-5: Back Pressure = 112 kPa).

V. CONCLUSIONS AND RECOMMENDATIONS

A. CONCLUSIONS

The present study validated the utility of the ICEM-CFD and CFX-5 codes. These codes will provide useful tools for future investigations into stall and surge of the transonic axial compressor. The ultimate goal is to provide means to investigate the "pop-stall" phenomenon.

ICEM-CFD and CFX-5 are commercial codes that have proven to be in reasonable agreement when compared to NASA's two codes. This code is particularly beneficial when its ability to operate in a "turbo" mode is considered. This feature allowed the user to generate a more accurate mesh with less time being spent on rotating points, curves, and surfaces to an exact position. Furthermore, the code results followed the trend of the experimental data. The results are encouraging considering that one-third fewer elements were being used than in the previous simulations.

B. RECOMMENDATIONS

It is recommended that the mesh be refined so that it more closely matches the grid size of the meshes used for the previous codes. This will ensure improved accuracy as well as eliminate any error associated with a course mesh.

Secondly, simulations should be run near stall conditions, and the results should be compared to experimental data to ascertain if the Ansys Inc. code can accurately model stall conditions. If it can then a full blade row simulation should be attempted to begin to map stall cells.

Finally, simulations need to be conducted to model the inlet distortion due to steam ingestion. CFX-5 can model various components simultaneously with great ease. The refined grid of BP7 along with the grids generated by Brunner (Brunner, 2005) should be merged to gain a comprehensive understanding of airflow and disruption through the rotor.

THIS PAGE INTENTIONALLY LEFT BLANK

LIST OF REFERENCES

1. Ansys.com, "Product Information", 2005, Canonsburg Pennsylvania.

2. Brunner, M.D., Comparison of Experimental and Computational Fluid Dynamics Measurements In A Transonic Compressor Inlet, Master's Thesis, Naval Postgraduate School, Monterey, California, September 2005.

3. Chima, R.V., 1998 "Calculation of Multistage Turbomachinery Using Steady Characteristics Boundary Layer Conditions," AIAA-98-0968 or NASA/TM - 1998-206613.

4. Donelson, S. Briggs, T., "*JSF Team Probes Steam Catapult Environment,*" JSF Integrated Test Force, dcmilitary.com, February 6, 2003.

5. Gannon, A.J., Hobson, G.V. and Shreeve, R.P., 2004, "A Transonic Compressor Stage Part 1: Experimental Results," ASME GT2004-53923, Turbo Expo, Vienna, Austria, June 14-17, 2004.

6. Gannon, A.J., Hobson, G.V. and Shreeve, R.P., 2005, "Measurement of the Unsteady Case Wall Pressures Over the Rotor of a Transonic Fan Stage and Comparison with Numerical Predictions," ISABE-2005-1099, Munich, Germany, September 4-9, 2005.

7. Harwell, www-Harwell.Ansys.com/demoroom, "Modeling Flow Around a Blade," 2005.

8. Hobson, , G.V., Gannon, A.J. and Shreeve, Raymond, R.P., 2004, "A Transonic Compressor Stage Part 2: CFD Simulation," ASME GT2004-53923, Turbo Expo, Vienna, Austria, June 14-17, 2004.

9. Hobson, G.V., Private Communications, 2005.

10. Jenping, C. and Hathaway, M., http://www.erc.msstate.edu/simcenter/docs/msturbo, 2005.

11. O'Brien, J.M., Transonic Compressor Test Rig Rebuild and Initial Results with Sanger Stage, Master's Thesis, Naval Postgraduate School, Monterey, California, June 2000.

12. Sanger, N.L., "Design of Low Aspect Ratio Transonic Compressor Stage Using CFD Techniques," ASME Journal of Turbomachinery, July 1996, Vol. 118 pp 479 – 491.

13. Sanger, N.L., "*Design Methodology for the NPS Transonic Compressor*," TPL Technical Note 99-01, Naval Postgraduate School, Monterey, California, August 1999.

14. Villescas, Ivan, Flow Field Surveys In A Transonic Compressor Prior To Inlet Steam Ingestion Tests, Master's Thesis, Naval Postgraduate School, Monterey, California, September 2005.

APPENDIX A: EXIT RELATIVE MACH NUMBER PROFILES

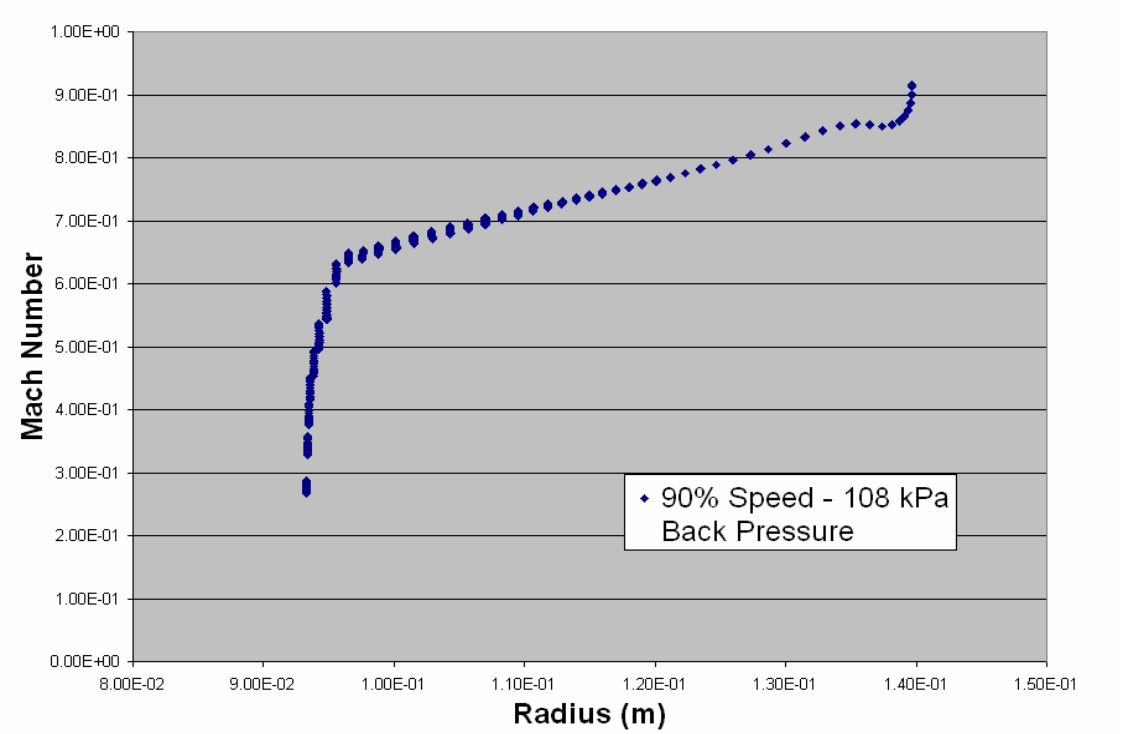

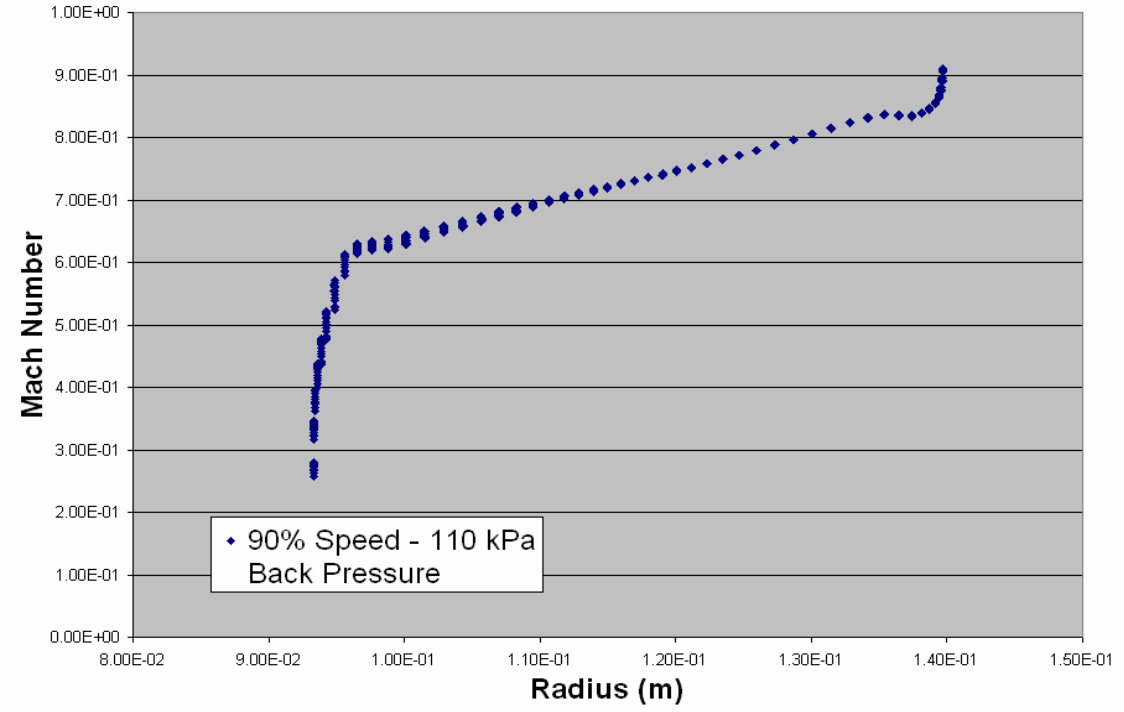

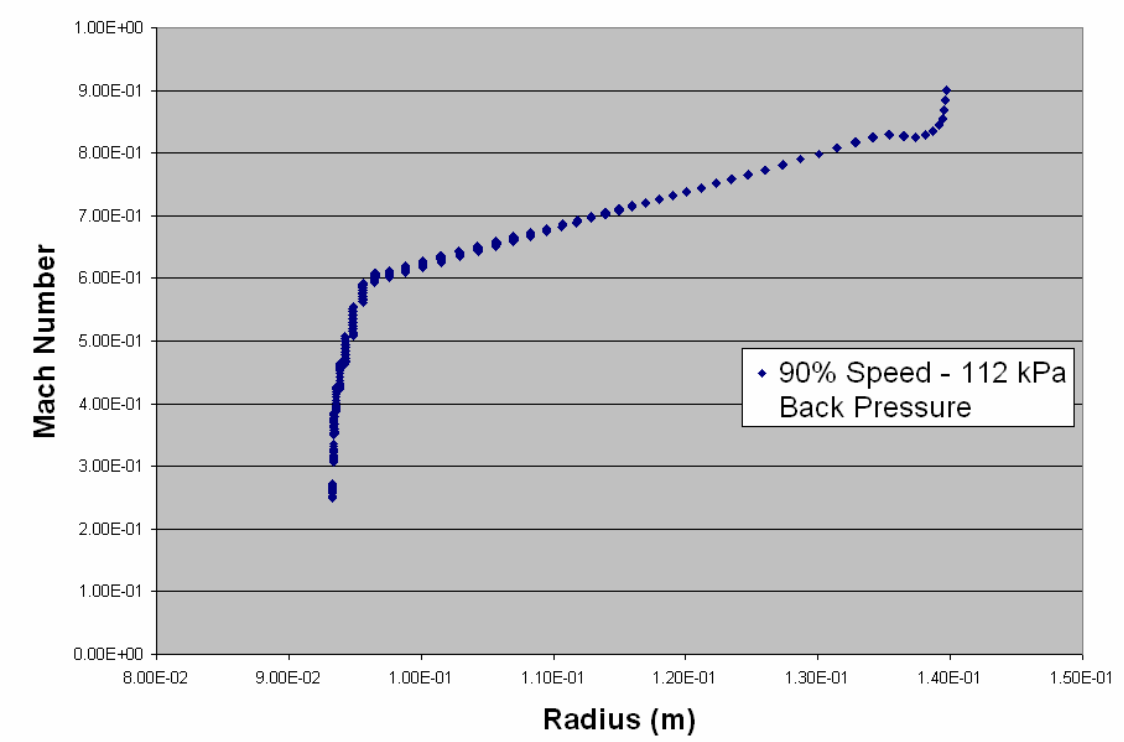
1.00E+00
9.00E-01
8.00E-01
7.00E-01
6.00E-01
5.00E-01
4.00E-01
3.00E-01
2.00E-01
1.00E-01
0.00E+00
Mach Number
8.00E-02
9.00E-02
1.00E-01
1.10E-01
1.20E-01
1.30E-01
1.40E-01
1.50E-01
Radius (m)
90% Speed - 112 kPa Back Pressure

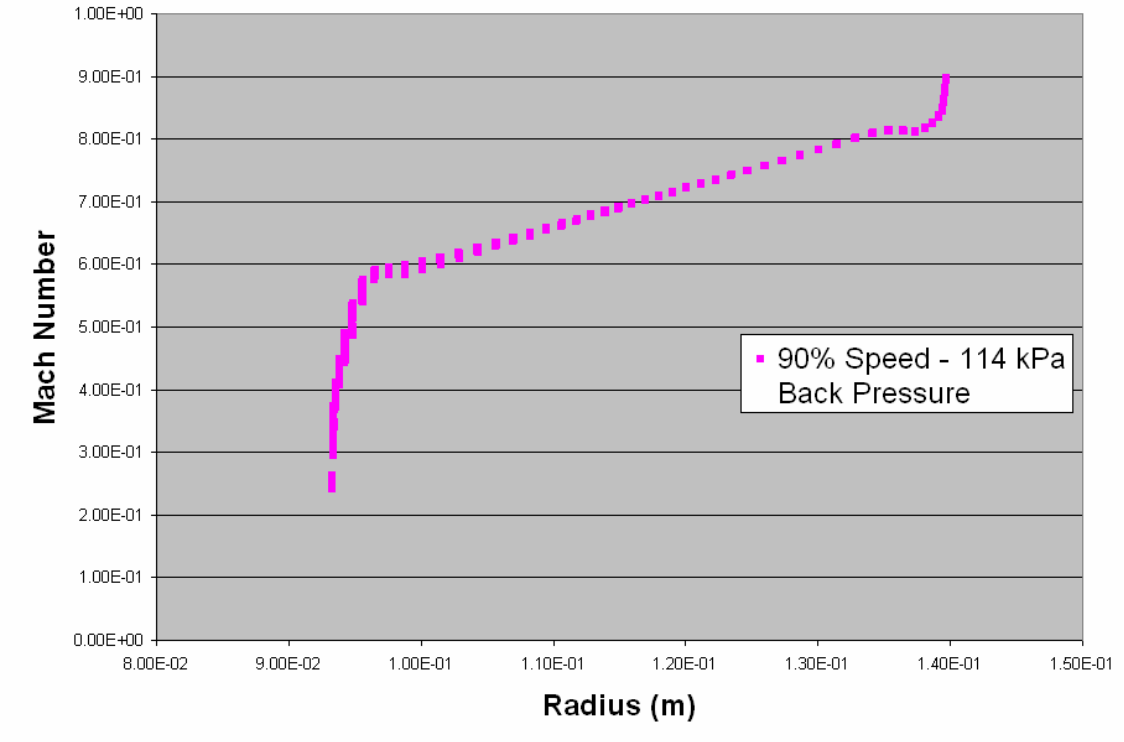
1.00E+00
9.00E-01
8.00E-01
7.00E-01
6.00E-01
5.00E-01
4.00E-01
3.00E-01
2.00E-01
1.00E-01
0.00E+00
Mach Number
8.00E-02
9.00E-02
1.00E-01
1.10E-01
1.20E-01
1.30E-01
1.40E-01
1.50E-01
Radius (m)
90% Speed - 114 kPa Back Pressure

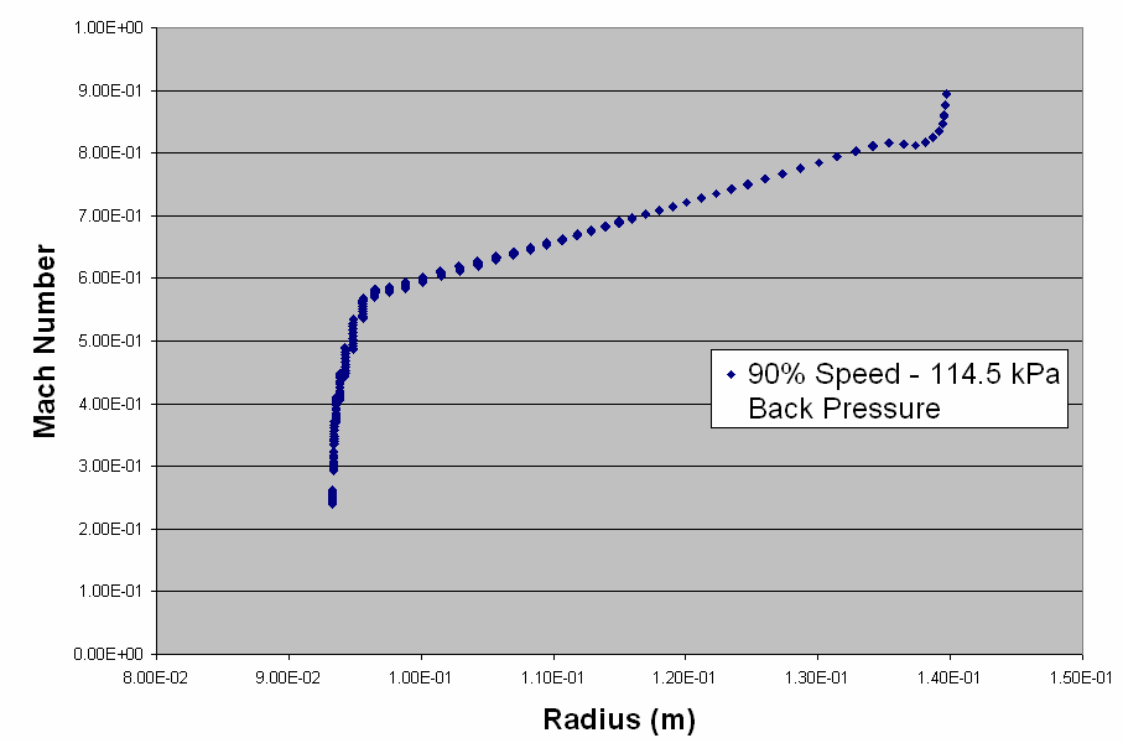
1.00E+00
9.00E-01
8.00E-01
7.00E-01
6.00E-01
5.00E-01
4.00E-01
3.00E-01
2.00E-01
1.00E-01
0.00E+00
Mach Number
8.00E-02
9.00E-02
1.00E-01
1.10E-01
1.20E-01
1.30E-01
1.40E-01
1.50E-01
Radius (m)
90% Speed - 114.5 kPa Back Pressure

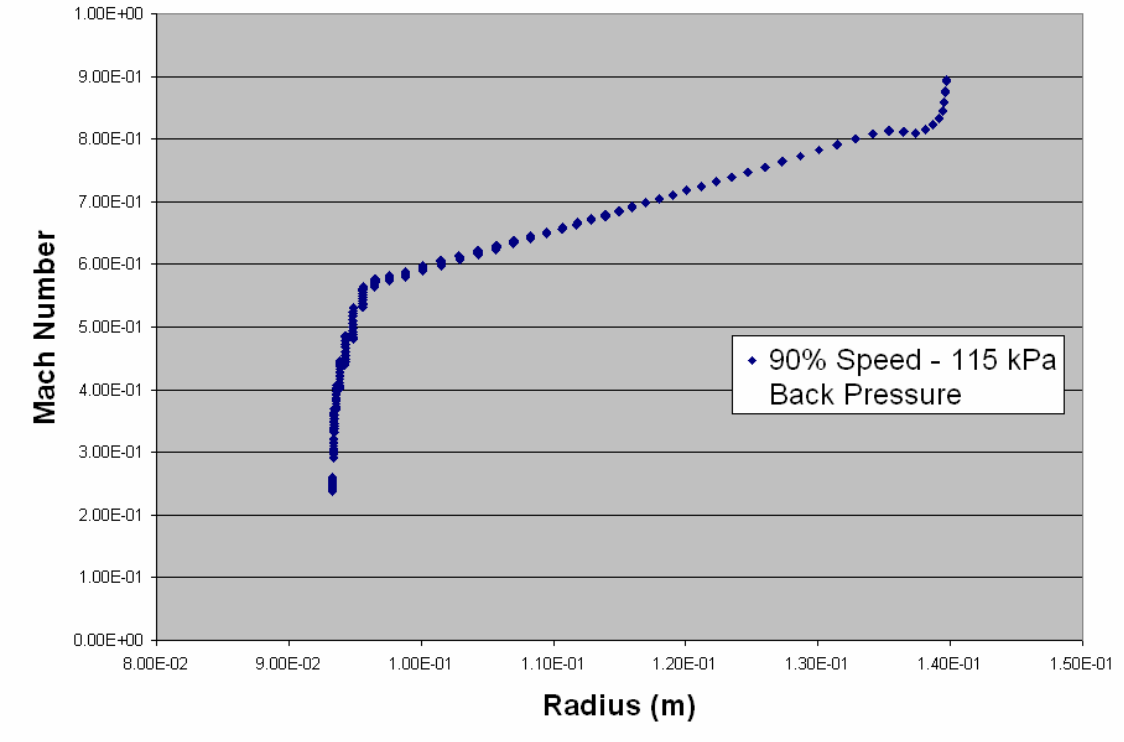
1.00E+00
9.00E-01
8.00E-01
7.00E-01
6.00E-01
5.00E-01
4.00E-01
3.00E-01
2.00E-01
1.00E-01
0.00E+00
Mach Number
8.00E-02
9.00E-02
1.00E-01
1.10E-01
1.20E-01
1.30E-01
1.40E-01
1.50E-01
Radius (m)
90% Speed - 115 kPa Back Pressure

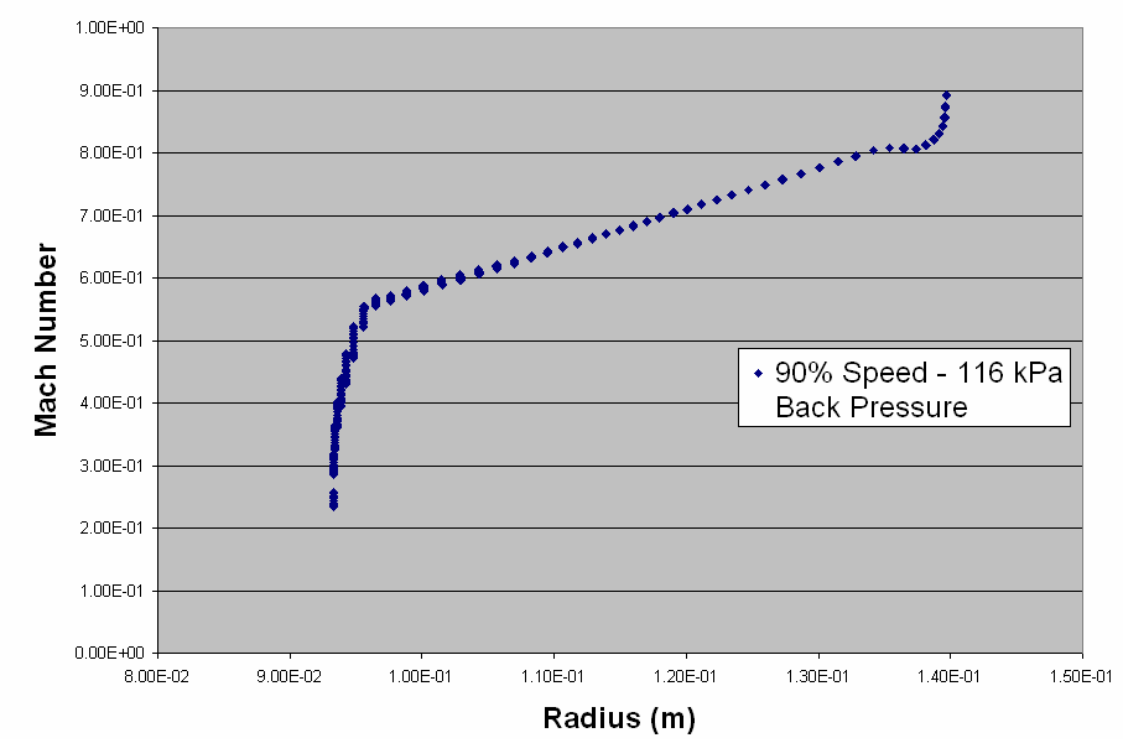
1.00E+00
9.00E-01
8.00E-01
7.00E-01
6.00E-01
5.00E-01
4.00E-01
3.00E-01
2.00E-01
1.00E-01
0.00E+00
Mach Number
8.00E-02
9.00E-02
1.00E-01
1.10E-01
1.20E-01
1.30E-01
1.40E-01
1.50E-01
Radius (m)
90% Speed - 116 kPa Back Pressure

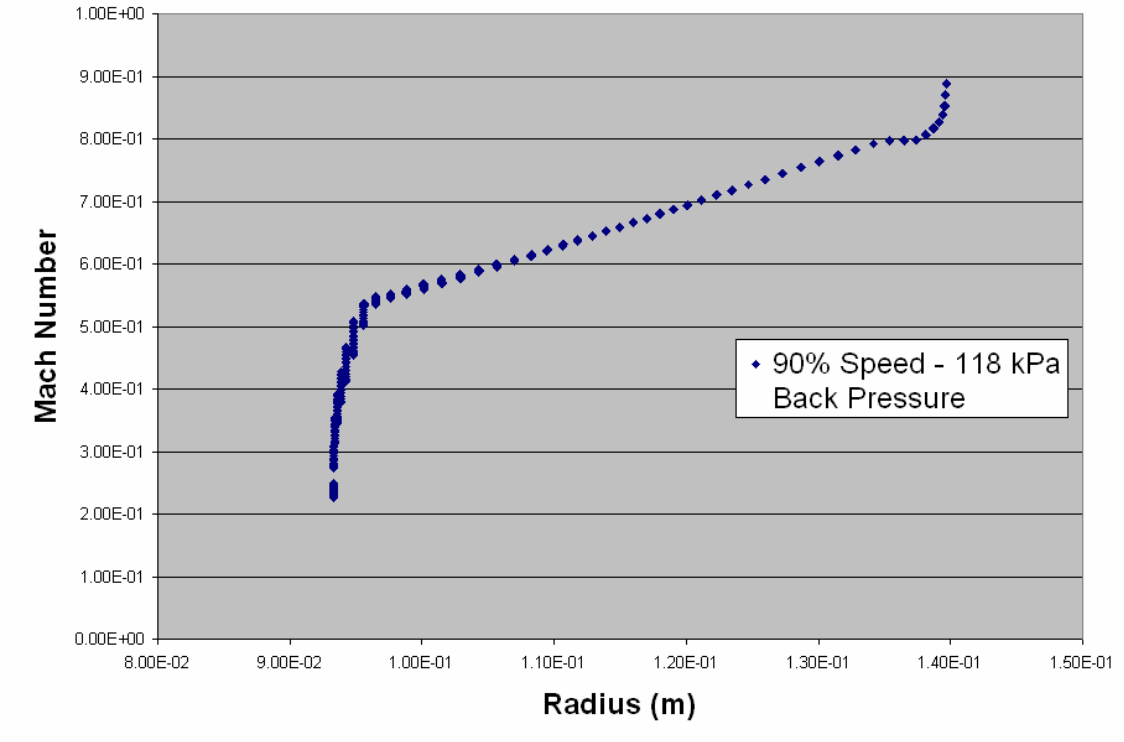
1.00E+00
9.00E-01
8.00E-01
7.00E-01
6.00E-01
5.00E-01
4.00E-01
3.00E-01
2.00E-01
1.00E-01
0.00E+00
Mach Number
8.00E-02
9.00E-02
1.00E-01
1.10E-01
1.20E-01
1.30E-01
1.40E-01
1.50E-01
Radius (m)
90% Speed - 118 kPa Back Pressure

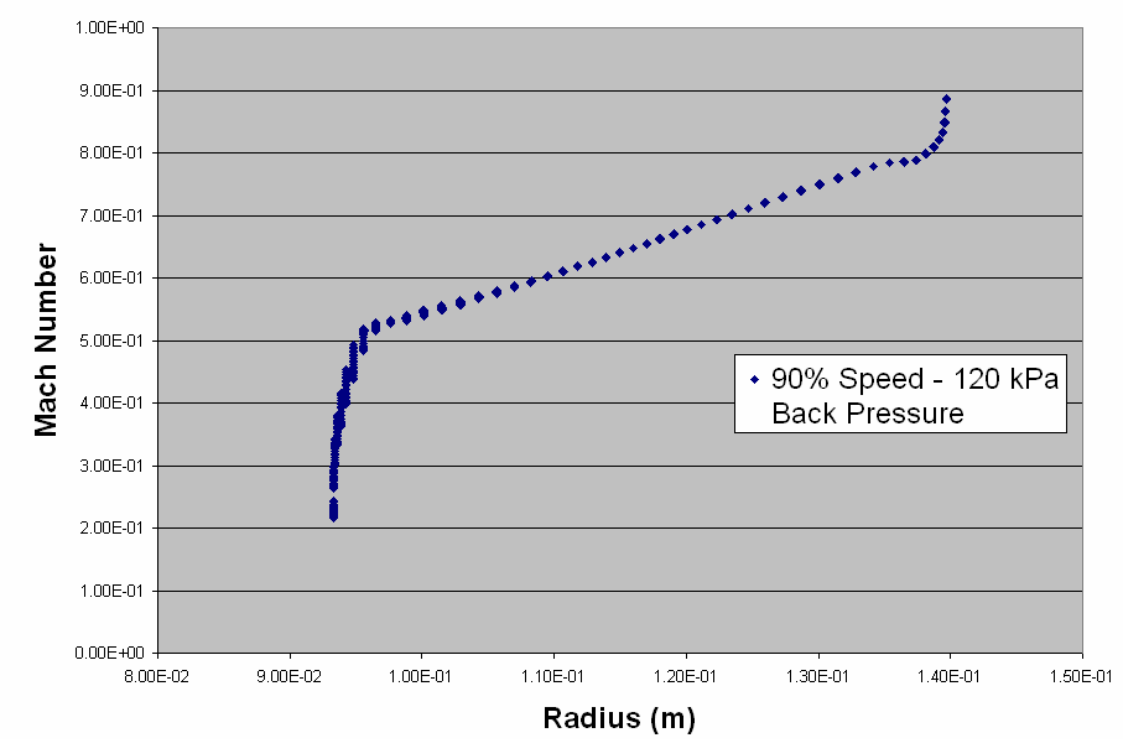
1.00E+00
9.00E-01
8.00E-01
7.00E-01
6.00E-01
5.00E-01
4.00E-01
3.00E-01
2.00E-01
1.00E-01
0.00E+00
Mach Number
8.00E-02
9.00E-02
1.00E-01
1.10E-01
1.20E-01
1.30E-01
1.40E-01
1.50E-01
Radius (m)
90% Speed - 120 kPa Back Pressure

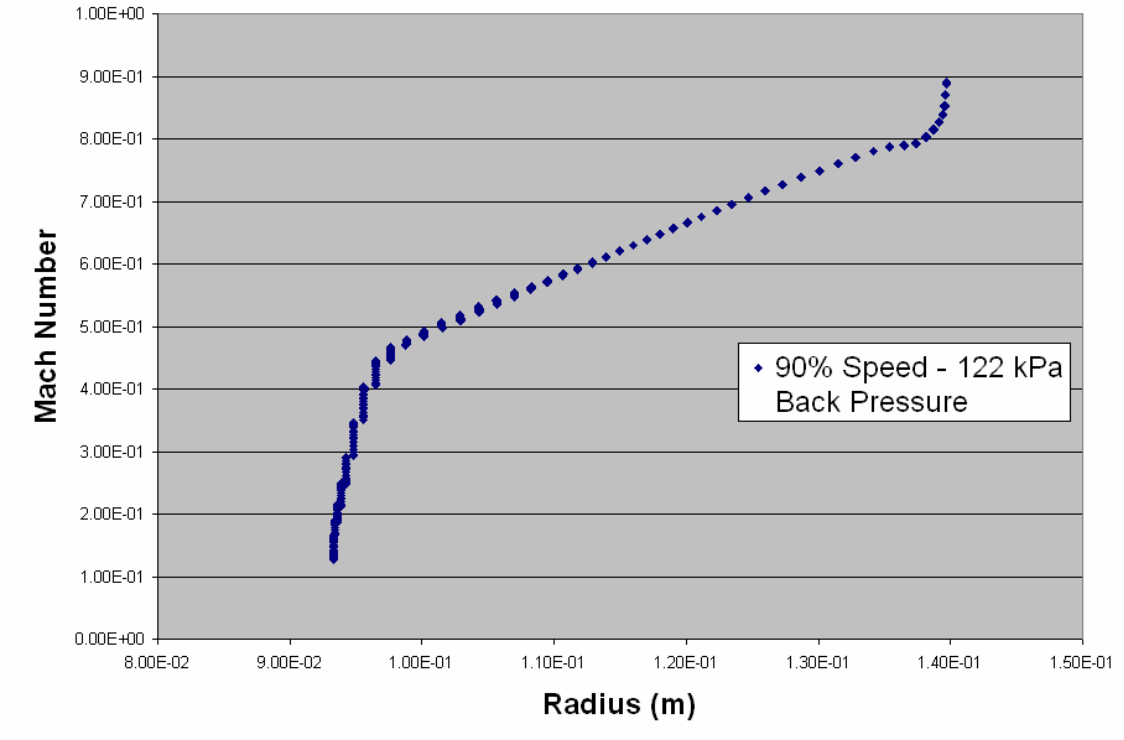
1.00E+00
9.00E-01
8.00E-01
7.00E-01
6.00E-01
5.00E-01
4.00E-01
3.00E-01
2.00E-01
1.00E-01
0.00E+00
Mach Number
8.00E-02
9.00E-02
1.00E-01
1.10E-01
1.20E-01
1.30E-01
1.40E-01
1.50E-01
Radius (m)
90% Speed - 122 kPa Back Pressure

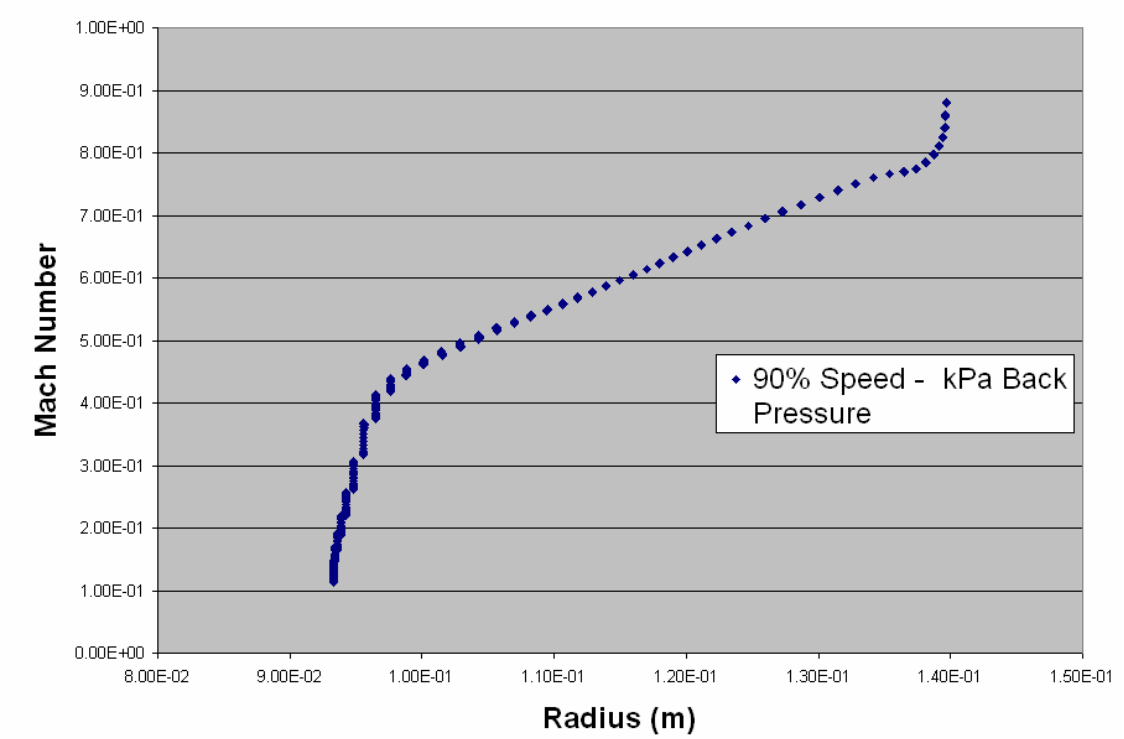
1.00E+00
9.00E-01
8.00E-01
7.00E-01
6.00E-01
5.00E-01
4.00E-01
3.00E-01
2.00E-01
1.00E-01
0.00E+00
Mach Number
8.00E-02
9.00E-02
1.00E-01
1.10E-01
1.20E-01
1.30E-01
1.40E-01
1.50E-01
Radius (m)
90% Speed - kPa Back Pressure

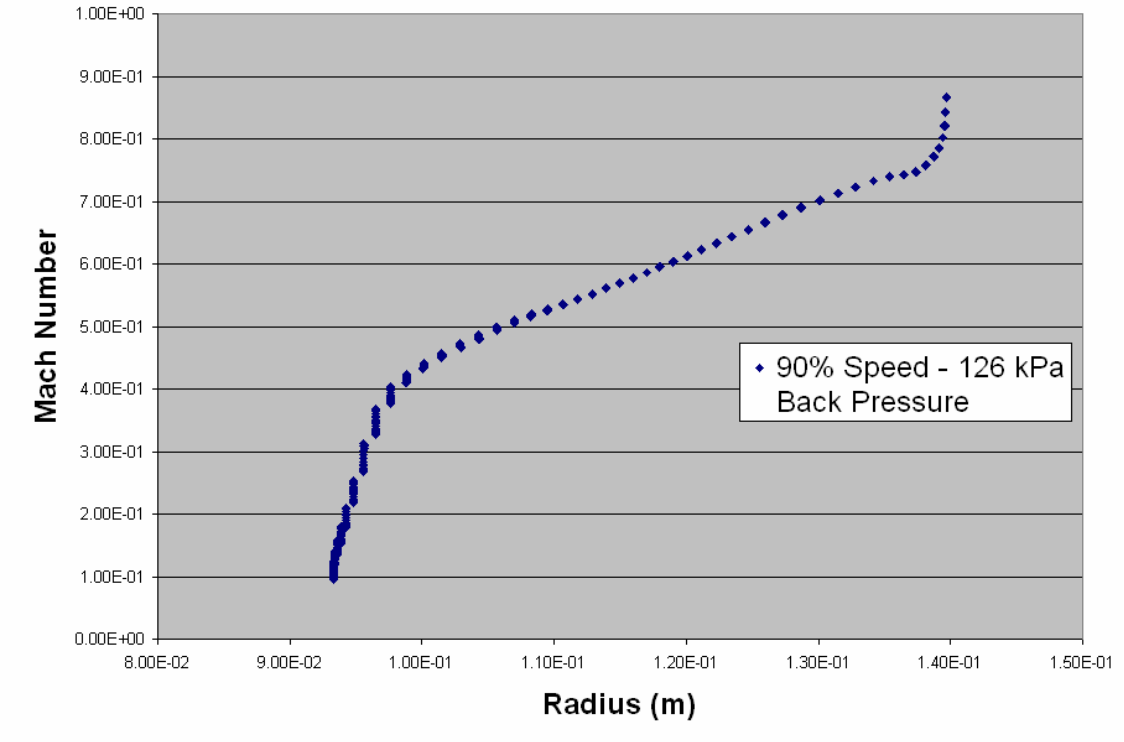
1.00E+00
9.00E-01
8.00E-01
7.00E-01
6.00E-01
5.00E-01
4.00E-01
3.00E-01
2.00E-01
1.00E-01
0.00E+00
Mach Number
8.00E-02
9.00E-02
1.00E-01
1.10E-01
1.20E-01
1.30E-01
1.40E-01
1.50E-01
Radius (m)
90% Speed - 126 kPa Back Pressure

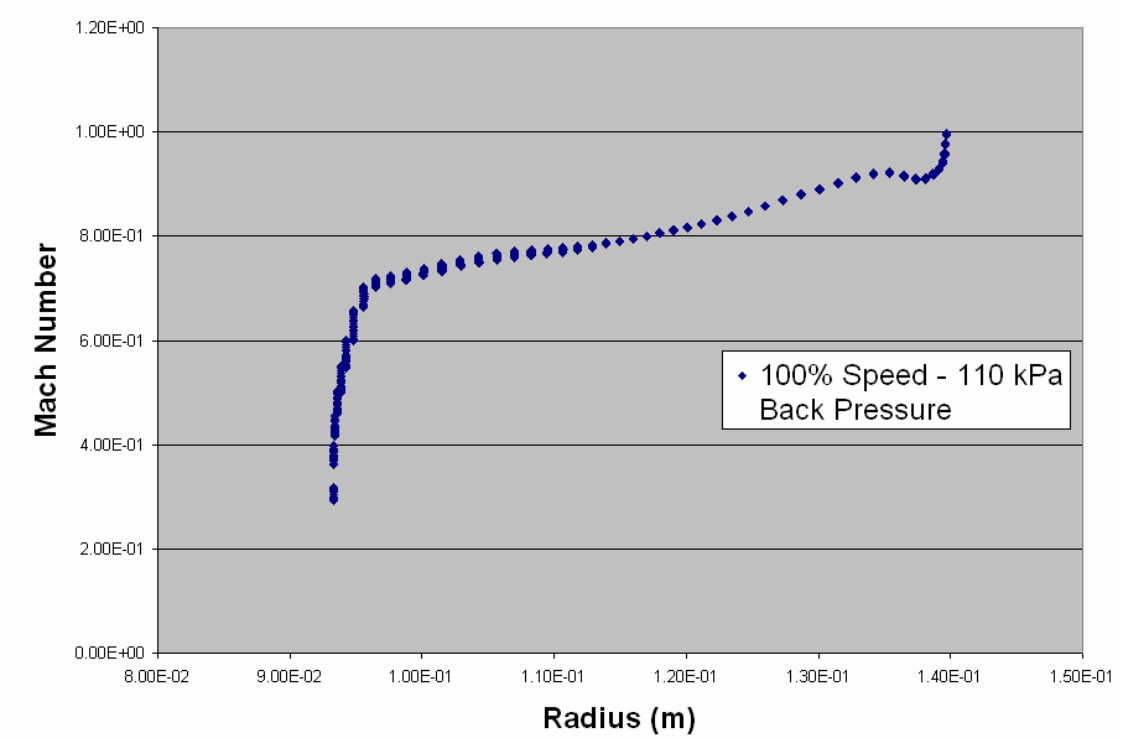
1.20E+00
1.00E+00
8.00E-01
6.00E-01
4.00E-01
2.00E-01
0.00E+00
Mach Number
8.00E-02
9.00E-02
1.00E-01
1.10E-01
1.20E-01
1.30E-01
1.40E-01
1.50E-01
Radius (m)
100% Speed - 110 kPa Back Pressure

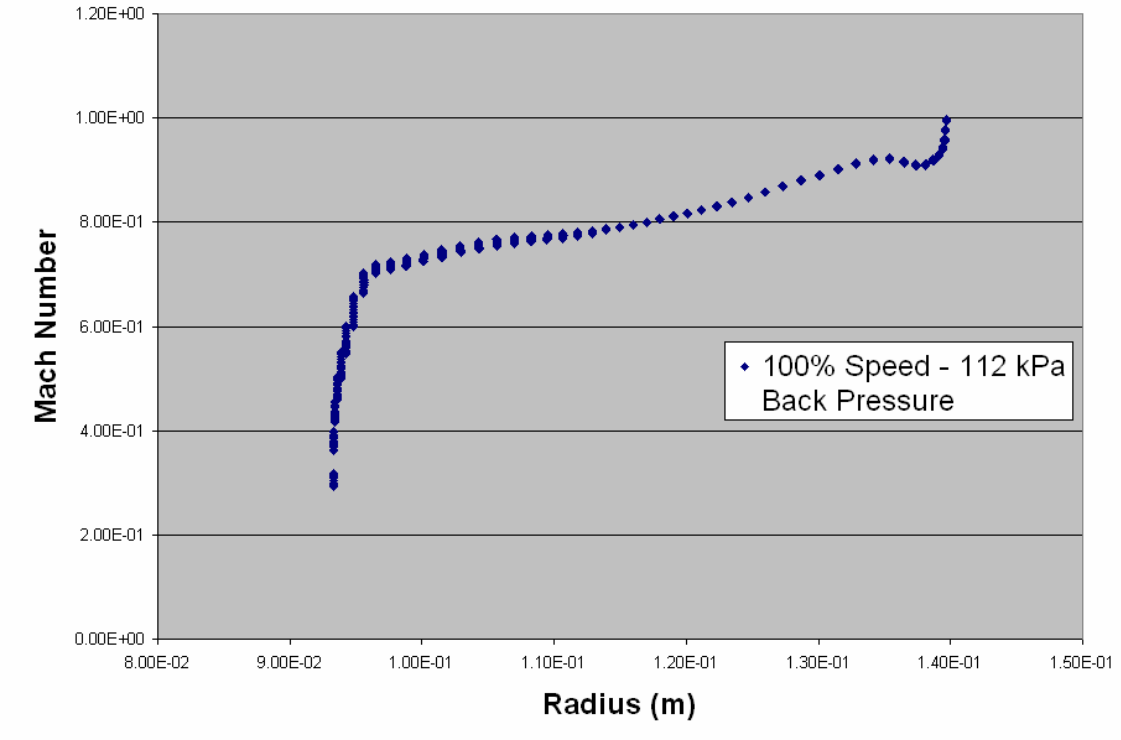
1.20E+00
1.00E+00
8.00E-01
6.00E-01
4.00E-01
2.00E-01
0.00E+00
Mach Number
8.00E-02
9.00E-02
1.00E-01
1.10E-01
1.20E-01
1.30E-01
1.40E-01
1.50E-01
Radius (m)
100% Speed - 112 kPa Back Pressure

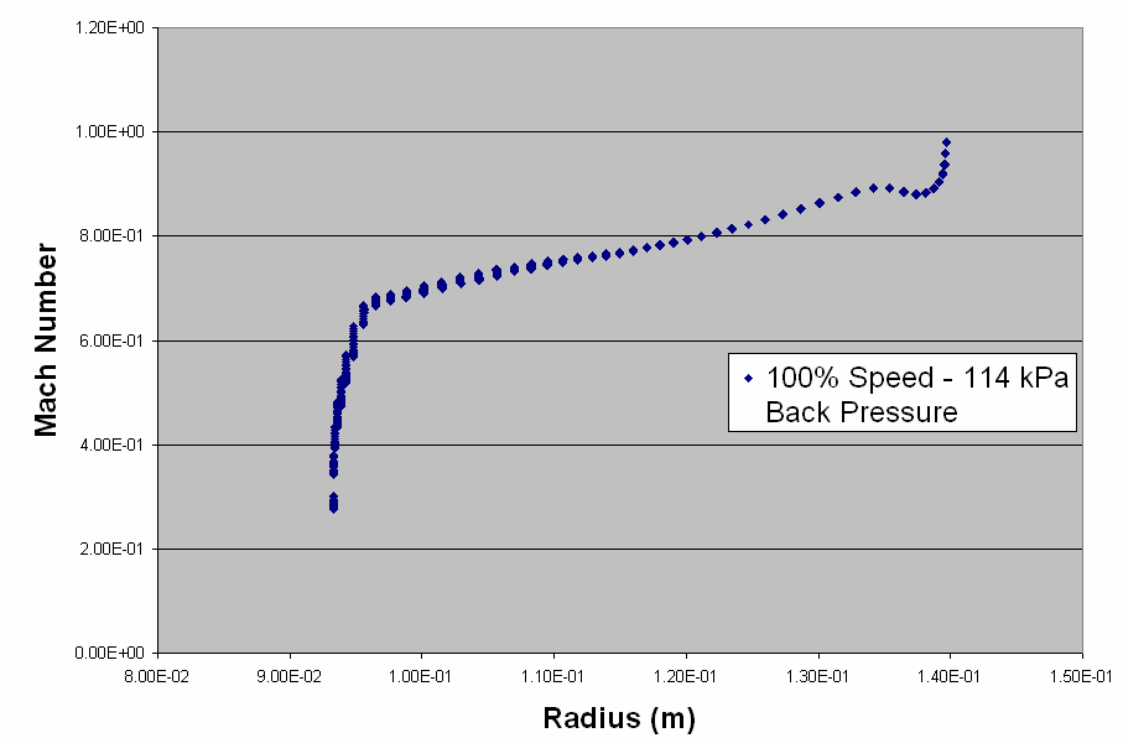
1.20E+00
1.00E+00
8.00E-01
6.00E-01
4.00E-01
2.00E-01
0.00E+00
Mach Number
8.00E-02
9.00E-02
1.00E-01
1.10E-01
1.20E-01
1.30E-01
1.40E-01
1.50E-01
Radius (m)
100% Speed - 114 kPa Back Pressure

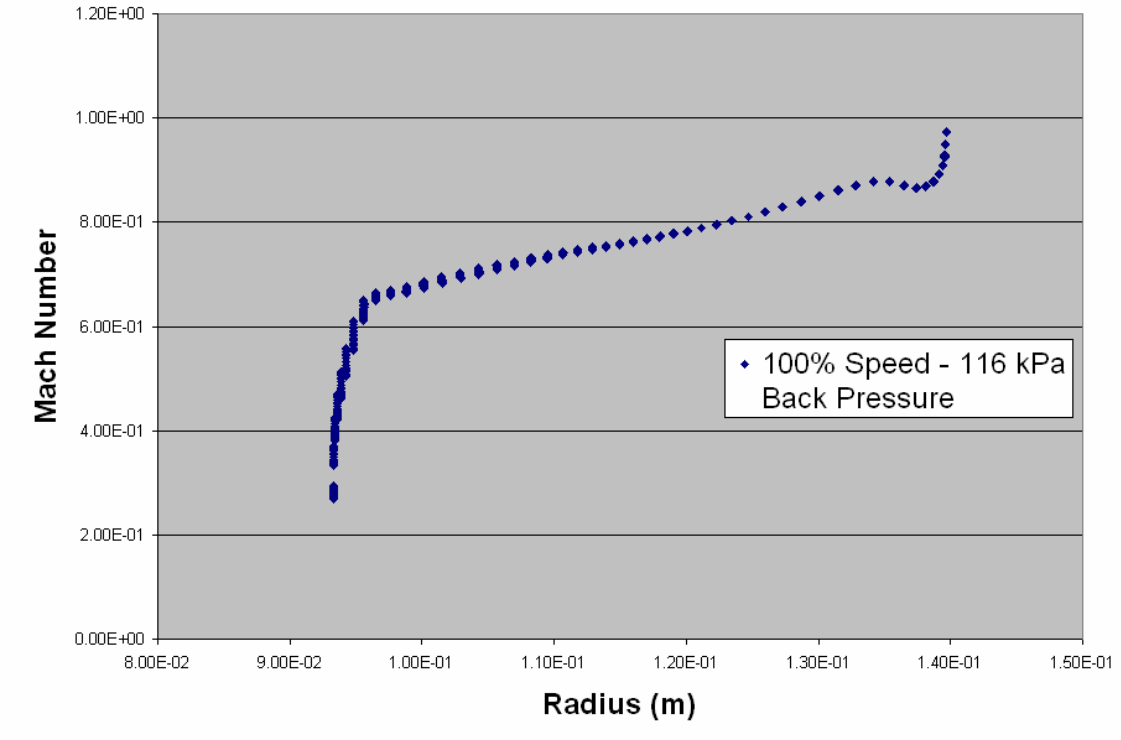
1.20E+00
1.00E+00
8.00E-01
6.00E-01
4.00E-01
2.00E-01
0.00E+00
Mach Number
8.00E-02
9.00E-02
1.00E-01
1.10E-01
1.20E-01
1.30E-01
1.40E-01
1.50E-01
Radius (m)
100% Speed - 116 kPa Back Pressure

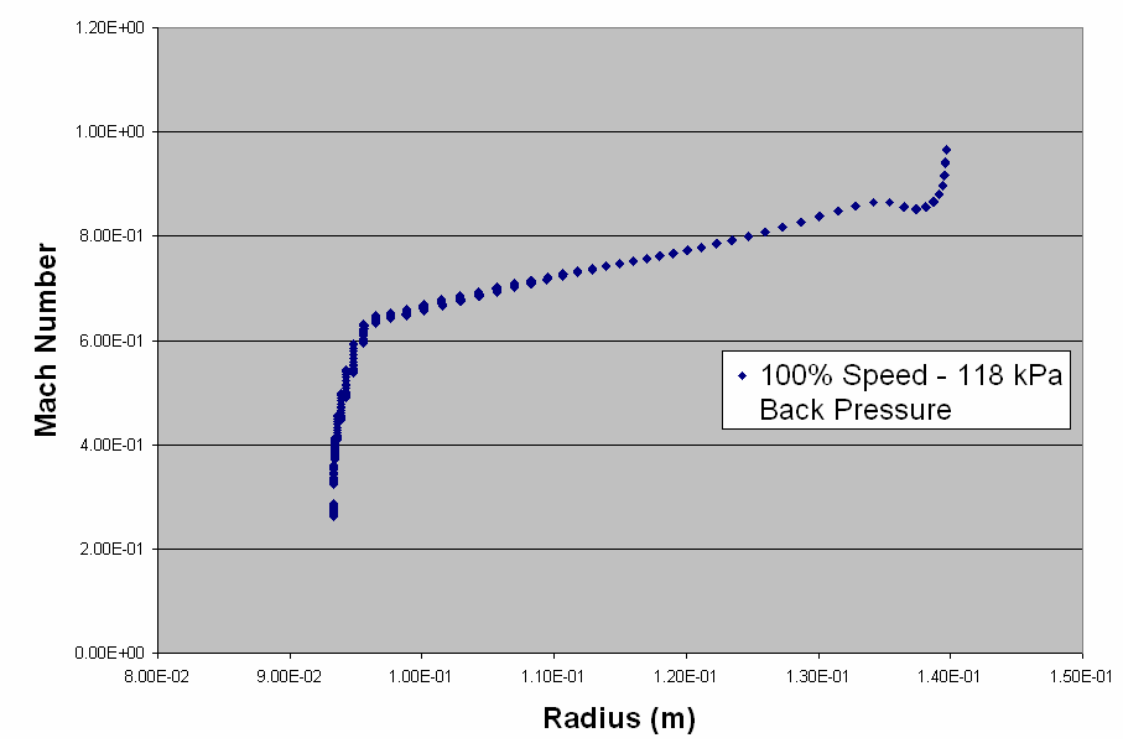
1.20E+00
1.00E+00
8.00E-01
6.00E-01
4.00E-01
2.00E-01
0.00E+00
Mach Number
8.00E-02
9.00E-02
1.00E-01
1.10E-01
1.20E-01
1.30E-01
1.40E-01
1.50E-01
Radius (m)
100% Speed - 118 kPa Back Pressure

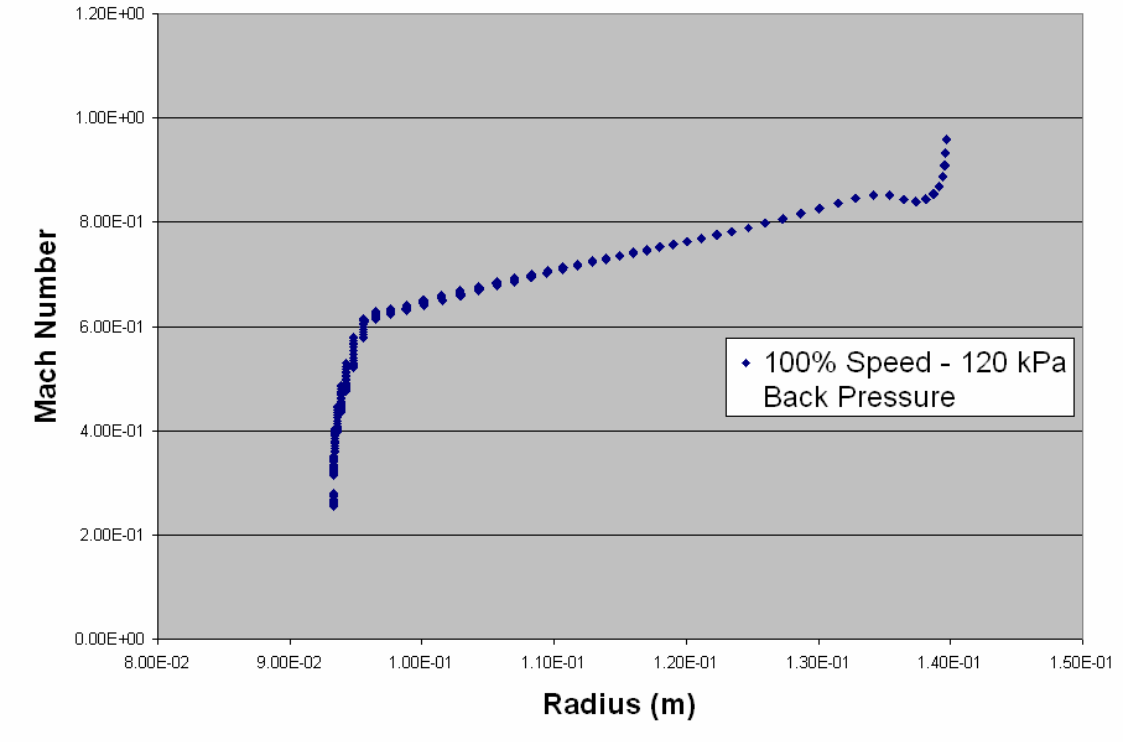
1.20E+00
1.00E+00
8.00E-01
6.00E-01
4.00E-01
2.00E-01
0.00E+00
Mach Number
8.00E-02
9.00E-02
1.00E-01
1.10E-01
1.20E-01
1.30E-01
1.40E-01
1.50E-01
Radius (m)
100% Speed - 120 kPa Back Pressure

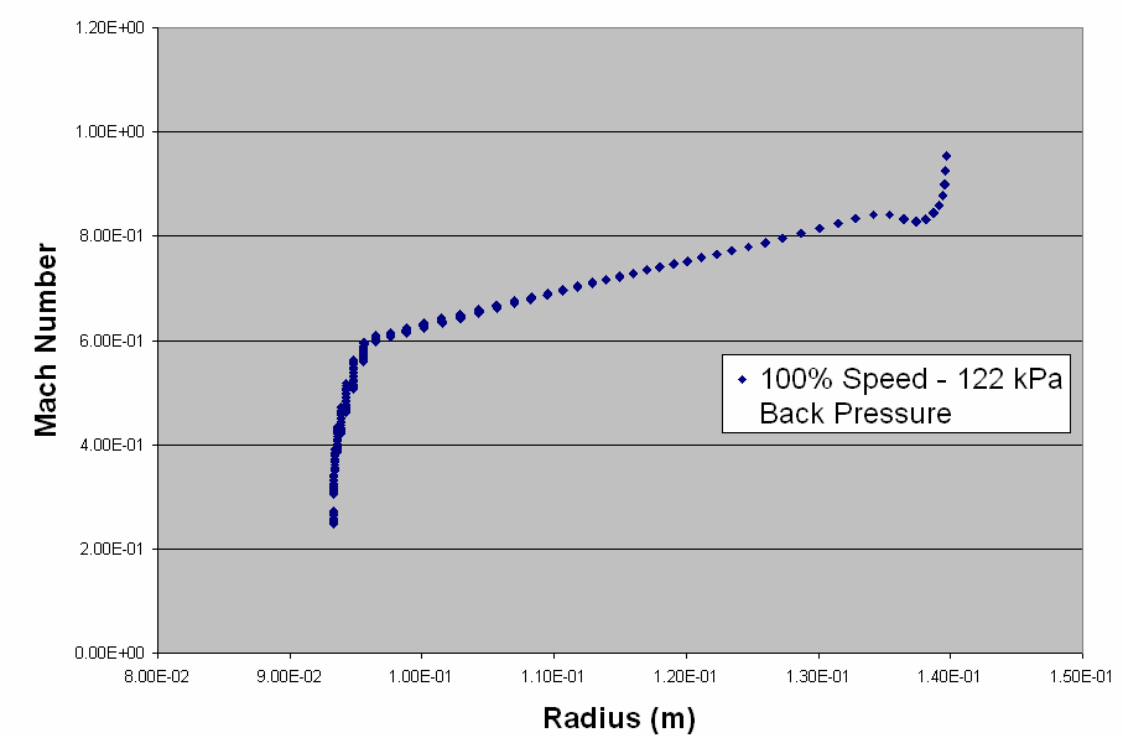
1.20E+00
1.00E+00
8.00E-01
6.00E-01
4.00E-01
2.00E-01
0.00E+00
Mach Number
8.00E-02
9.00E-02
1.00E-01
1.10E-01
1.20E-01
1.30E-01
1.40E-01
1.50E-01
Radius (m)
100% Speed - 122 kPa Back Pressure

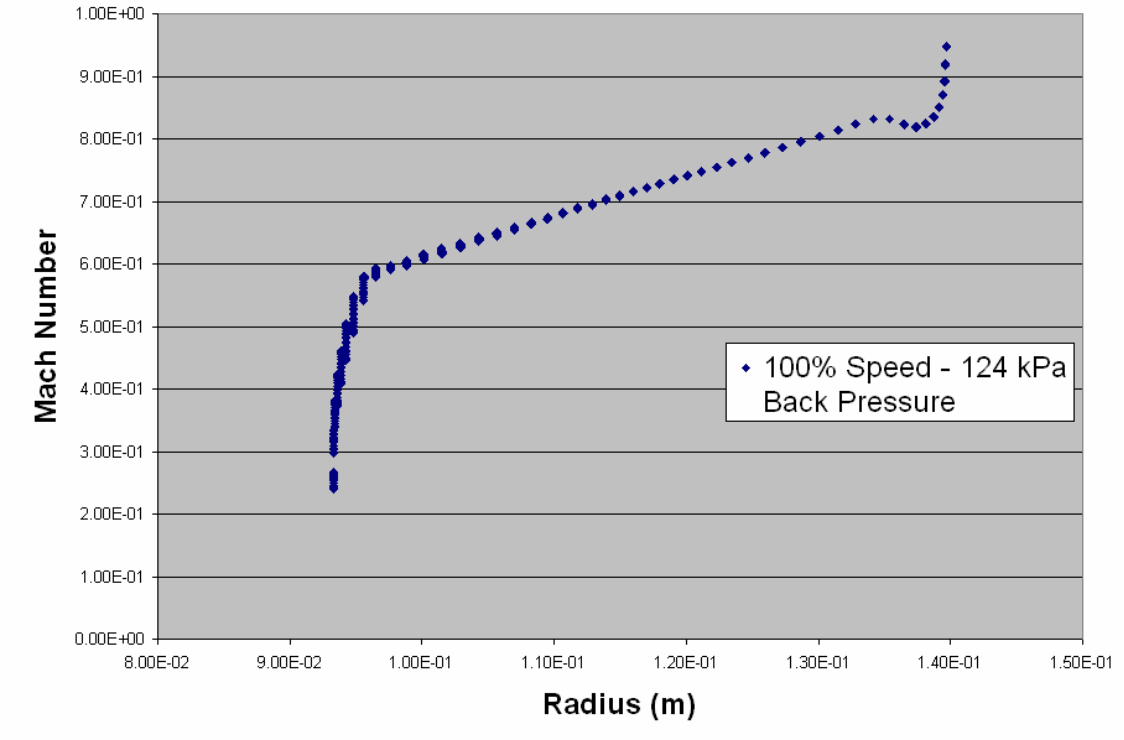
1.00E+00
9.00E-01
8.00E-01
7.00E-01
6.00E-01
5.00E-01
4.00E-01
3.00E-01
2.00E-01
1.00E-01
0.00E+00
Mach Number
8.00E-02
9.00E-02
1.00E-01
1.10E-01
1.20E-01
1.30E-01
1.40E-01
1.50E-01
Radius (m)
100% Speed - 124 kPa Back Pressure

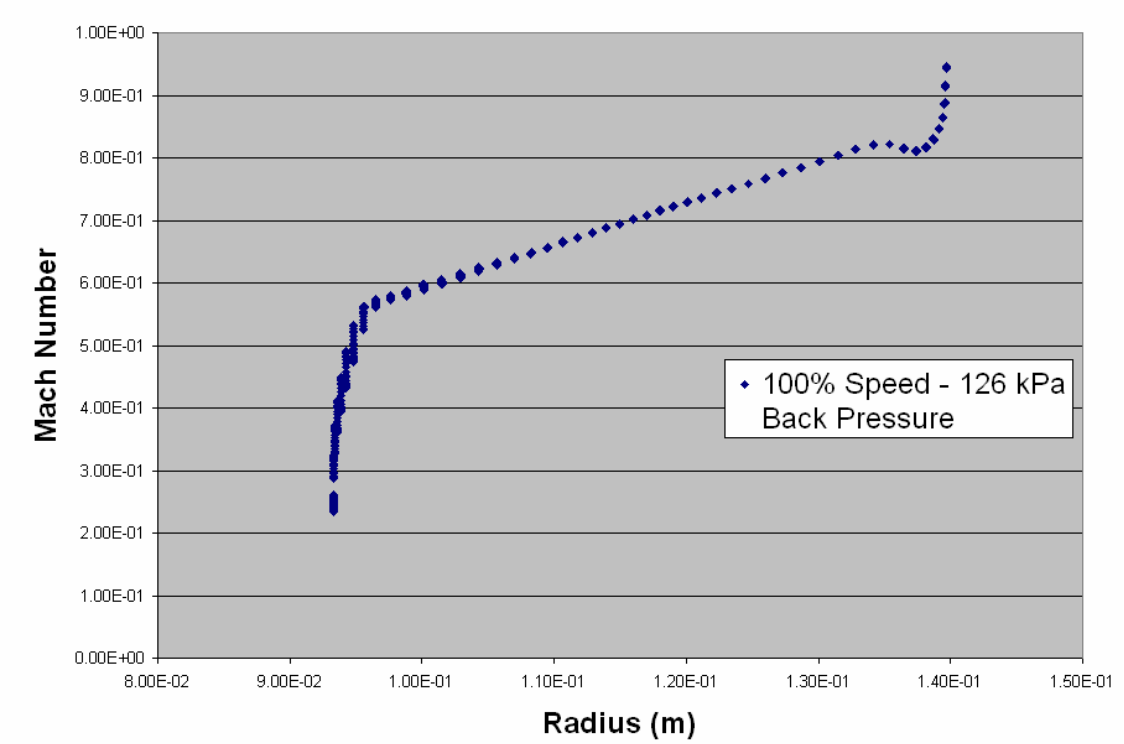
1.00E+00
9.00E-01
8.00E-01
7.00E-01
6.00E-01
5.00E-01
4.00E-01
3.00E-01
2.00E-01
1.00E-01
0.00E+00
Mach Number
8.00E-02
9.00E-02
1.00E-01
1.10E-01
1.20E-01
1.30E-01
1.40E-01
1.50E-01
Radius (m)
100% Speed - 126 kPa Back Pressure

THIS PAGE INTENTIONALLY LEFT BLANK

APPENDIX B: EXIT STAGNATION PRESSURE PROFILES

(Reference Pressure = 101 kPa)

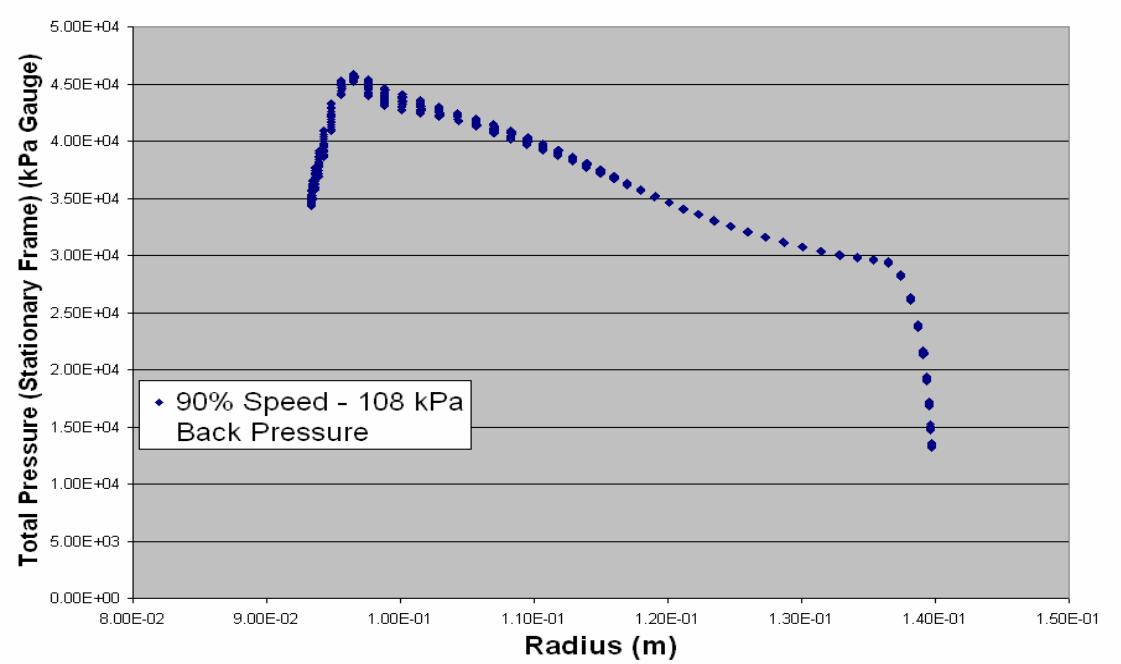

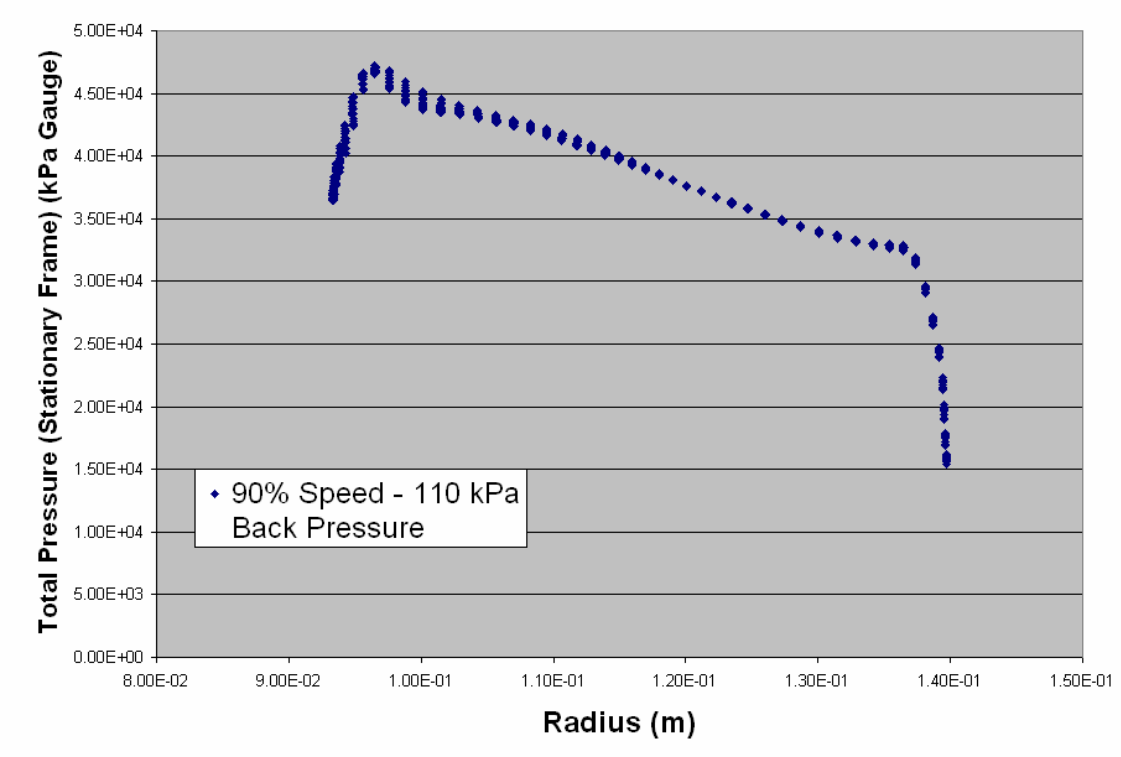

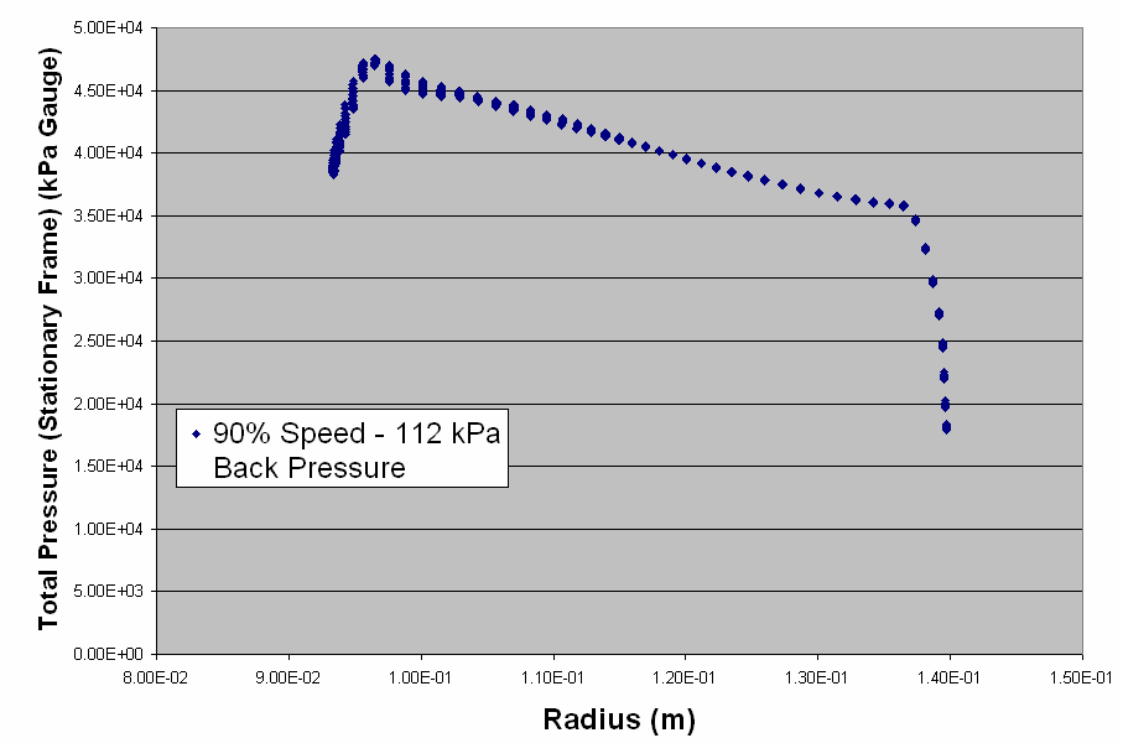
Total Pressure (Stationary Frame) (kPa Gauge)
5.00E+04
4.50E+04
4.00E+04
3.50E+04
3.00E+04
2.50E+04
2.00E+04
1.50E+04
1.00E+04
5.00E+03
0.00E+00
8.00E-02
9.00E-02
1.00E-01
1.10E-01
1.20E-01
1.30E-01
1.40E-01
1.50E-01
Radius (m)
90% Speed - 112 kPa Back Pressure

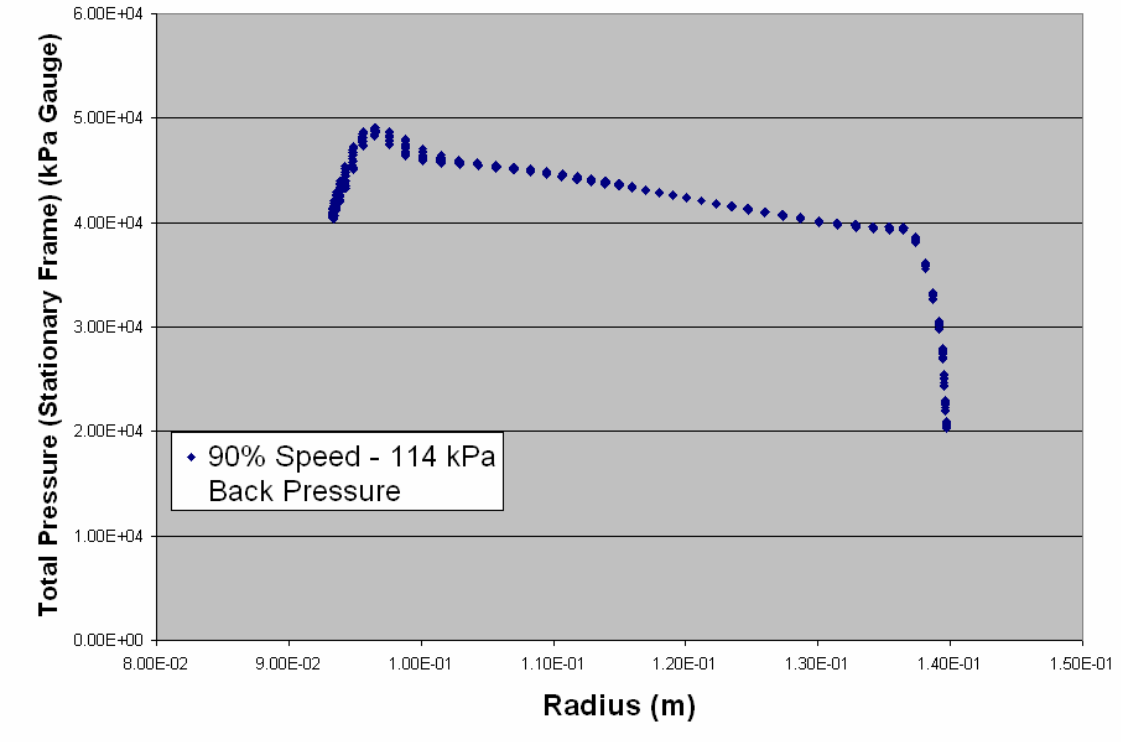
Total Pressure (Stationary Frame) (kPa Gauge)
6.00E+04
5.00E+04
4.00E+04
3.00E+04
2.00E+04
1.00E+04
0.00E+00
8.00E-02
9.00E-02
1.00E-01
1.10E-01
1.20E-01
1.30E-01
1.40E-01
1.50E-01
Radius (m)
90% Speed - 114 kPa Back Pressure

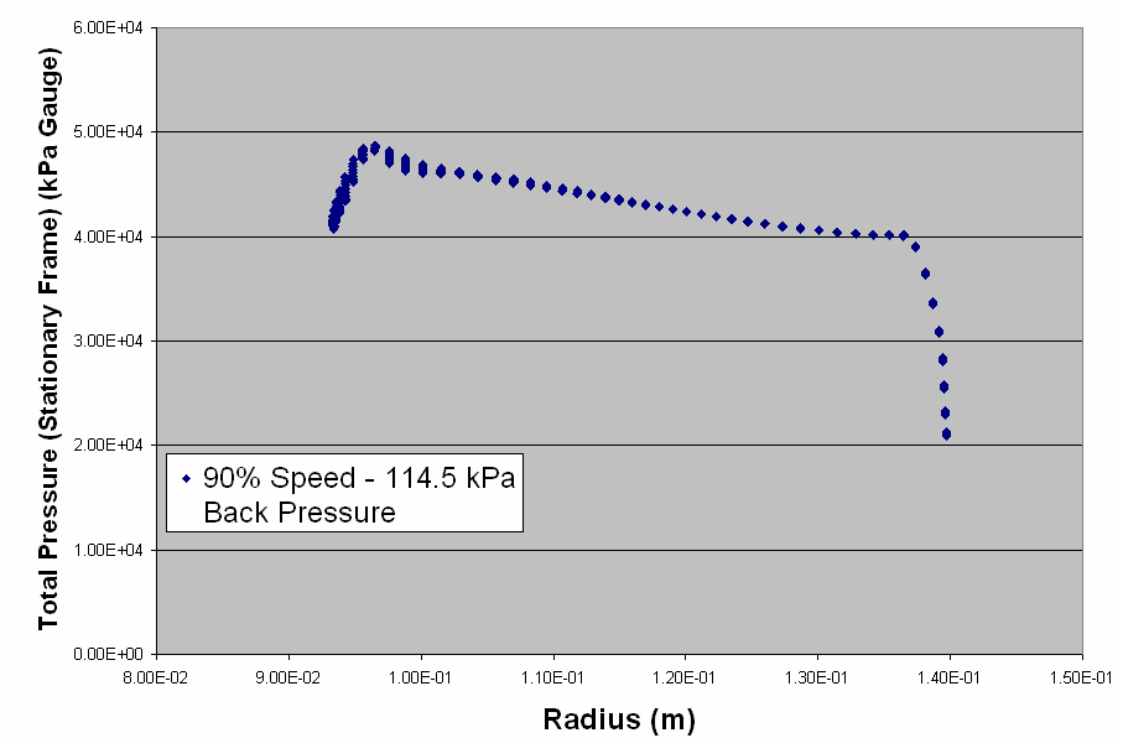
Total Pressure (Stationary Frame) (kPa Gauge)
6.00E+04
5.00E+04
4.00E+04
3.00E+04
2.00E+04
1.00E+04
0.00E+00
8.00E-02
9.00E-02
1.00E-01
1.10E-01
1.20E-01
1.30E-01
1.40E-01
1.50E-01
Radius (m)
90% Speed - 114.5 kPa Back Pressure

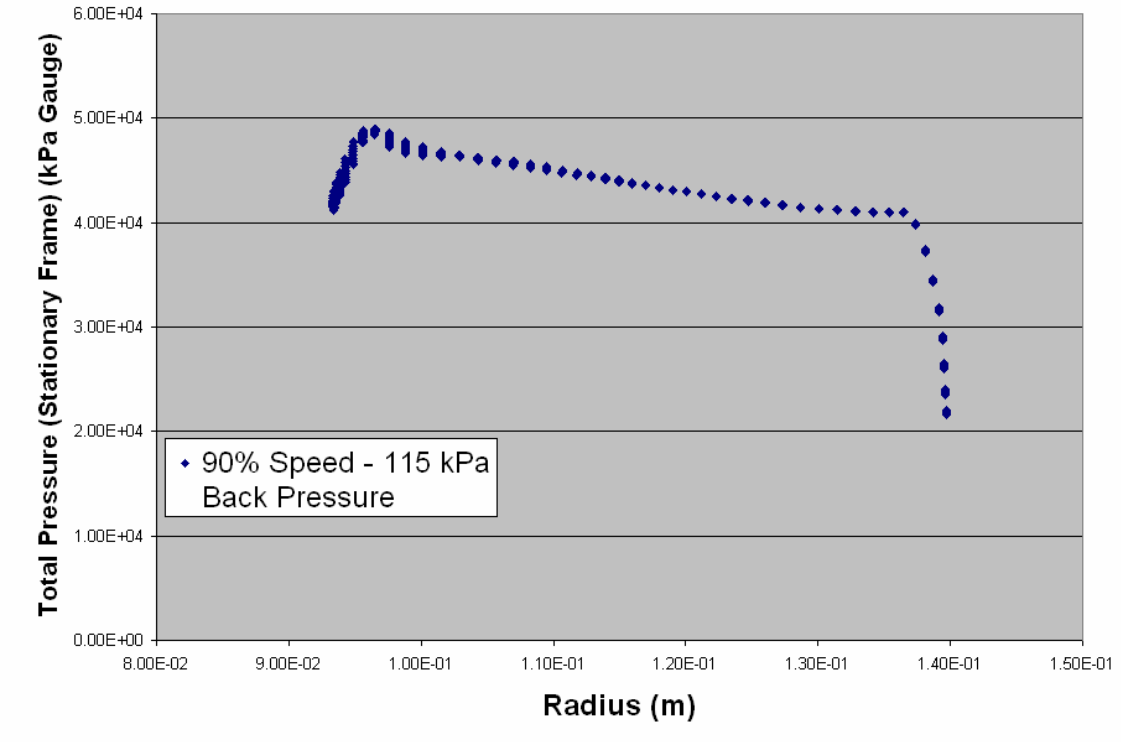
Total Pressure (Stationary Frame) (kPa Gauge)
6.00E+04
5.00E+04
4.00E+04
3.00E+04
2.00E+04
1.00E+04
0.00E+00
8.00E-02
9.00E-02
1.00E-01
1.10E-01
1.20E-01
1.30E-01
1.40E-01
1.50E-01
Radius (m)
90% Speed - 115 kPa Back Pressure

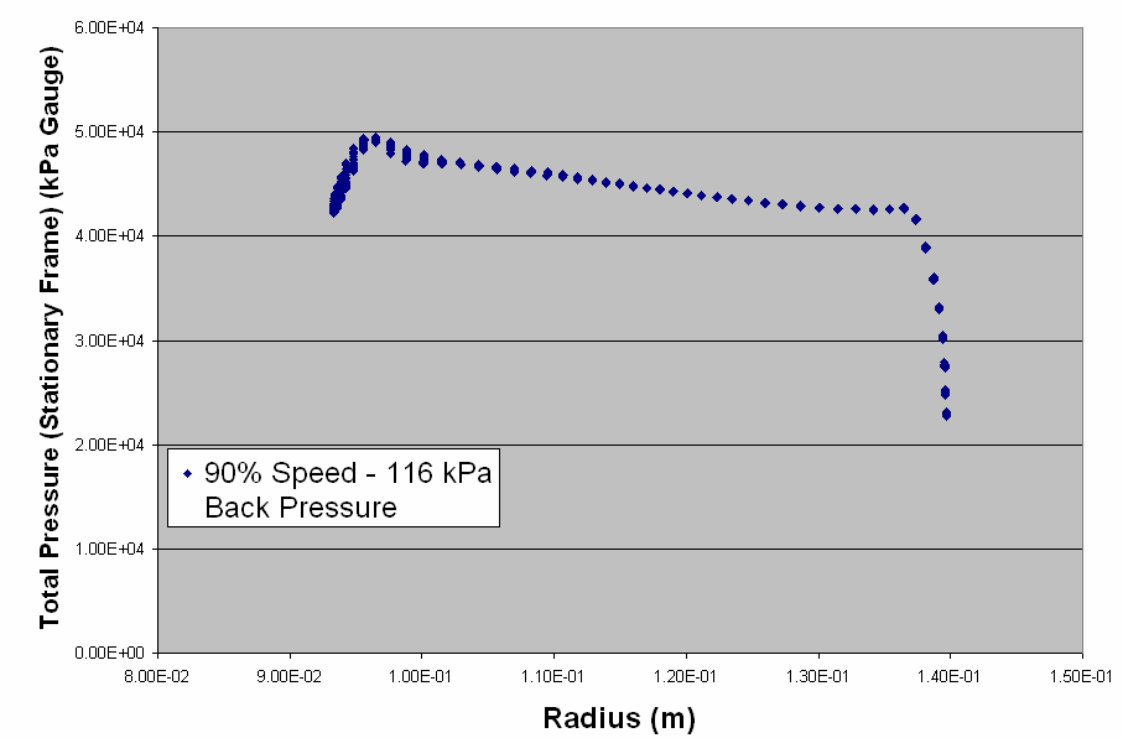
Total Pressure (Stationary Frame) (kPa Gauge)
6.00E+04
5.00E+04
4.00E+04
3.00E+04
2.00E+04
1.00E+04
0.00E+00
8.00E-02
9.00E-02
1.00E-01
1.10E-01
1.20E-01
1.30E-01
1.40E-01
1.50E-01
Radius (m)
90% Speed - 116 kPa Back Pressure

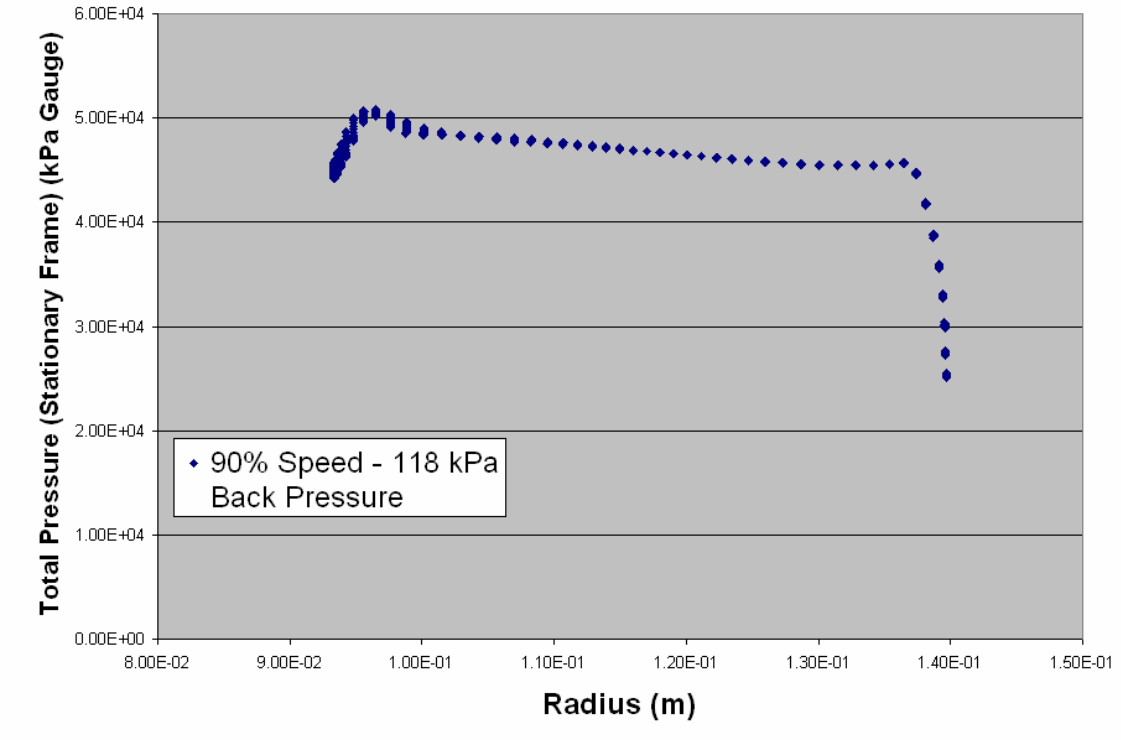
Total Pressure (Stationary Frame) (kPa Gauge)
6.00E+04
5.00E+04
4.00E+04
3.00E+04
2.00E+04
1.00E+04
0.00E+00
8.00E-02
9.00E-02
1.00E-01
1.10E-01
1.20E-01
1.30E-01
1.40E-01
1.50E-01
Radius (m)
90% Speed - 118 kPa Back Pressure

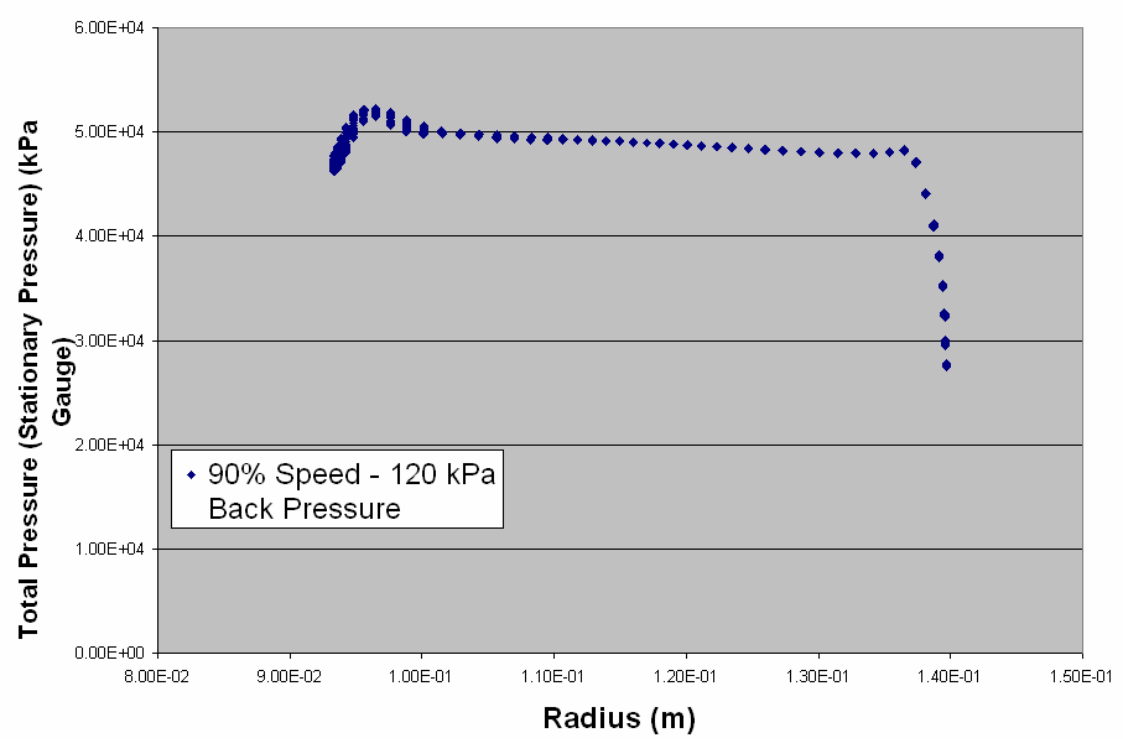
Total Pressure (Stationary Pressure) (kPa Gauge)
6.00E+04
5.00E+04
4.00E+04
3.00E+04
2.00E+04
1.00E+04
0.00E+00
8.00E-02
9.00E-02
1.00E-01
1.10E-01
1.20E-01
1.30E-01
1.40E-01
1.50E-01
Radius (m)
90% Speed - 120 kPa Back Pressure

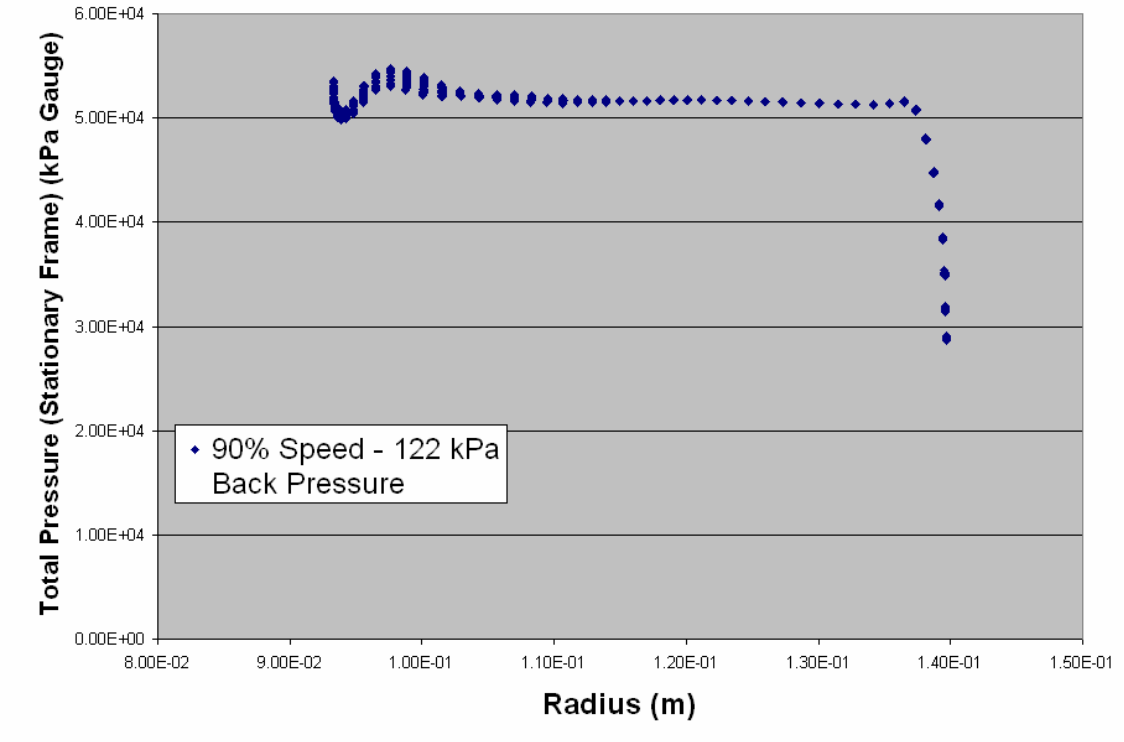
Total Pressure (Stationary Frame) (kPa Gauge)
6.00E+04
5.00E+04
4.00E+04
3.00E+04
2.00E+04
1.00E+04
0.00E+00
8.00E-02
9.00E-02
1.00E-01
1.10E-01
1.20E-01
1.30E-01
1.40E-01
1.50E-01
Radius (m)
90% Speed - 122 kPa Back Pressure

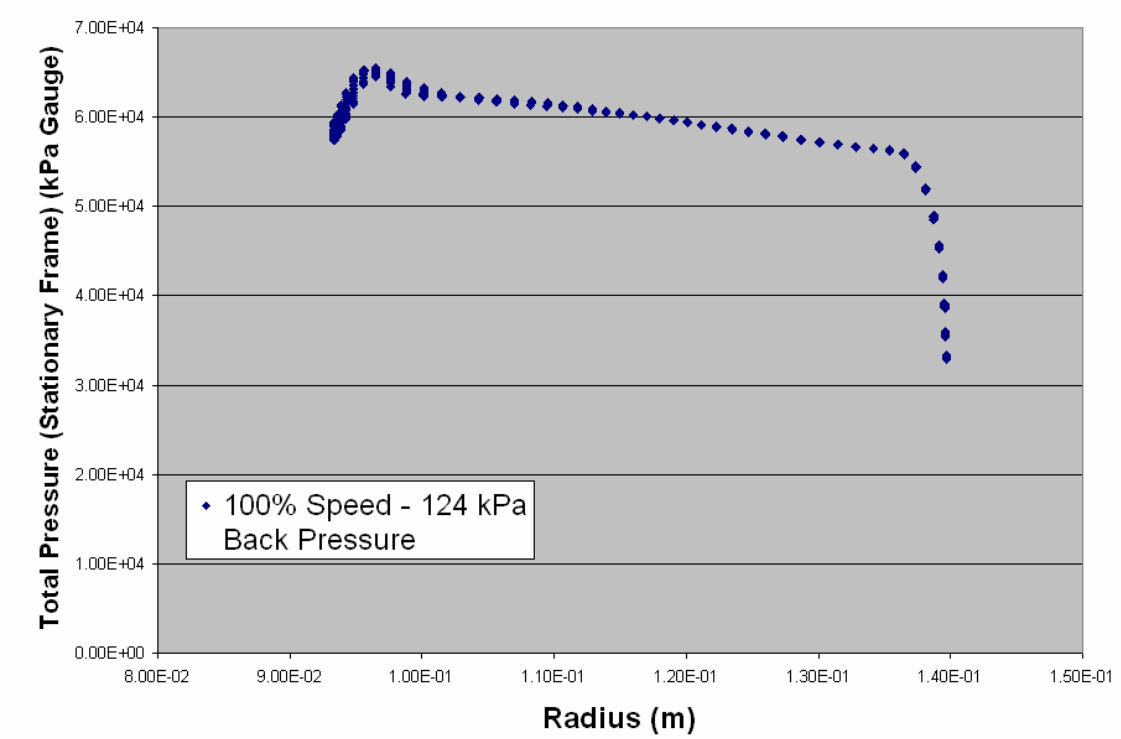
Total Pressure (Stationary Frame) (kPa Gauge)
7.00E+04
6.00E+04
5.00E+04
4.00E+04
3.00E+04
2.00E+04
1.00E+04
0.00E+00
8.00E-02
9.00E-02
1.00E-01
1.10E-01
1.20E-01
1.30E-01
1.40E-01
1.50E-01
Radius (m)
100% Speed - 124 kPa Back Pressure

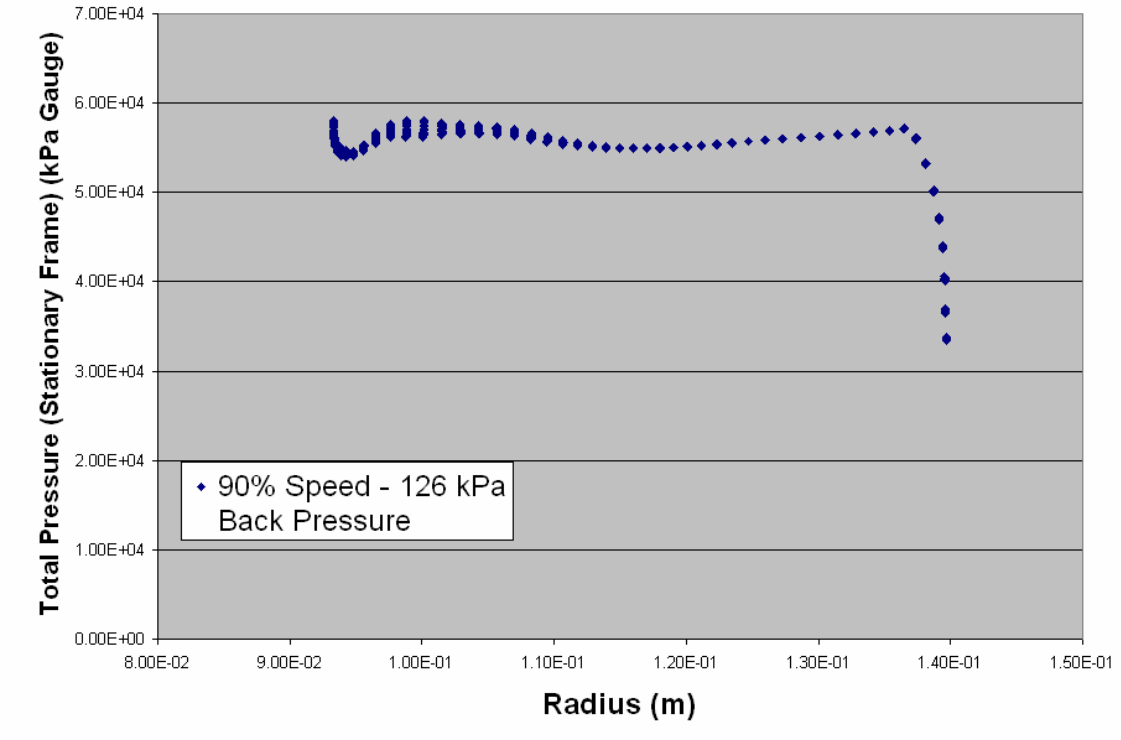
Total Pressure (Stationary Frame) (kPa Gauge)
7.00E+04
6.00E+04
5.00E+04
4.00E+04
3.00E+04
2.00E+04
1.00E+04
0.00E+00
8.00E-02
9.00E-02
1.00E-01
1.10E-01
1.20E-01
1.30E-01
1.40E-01
1.50E-01
Radius (m)
90% Speed - 126 kPa Back Pressure

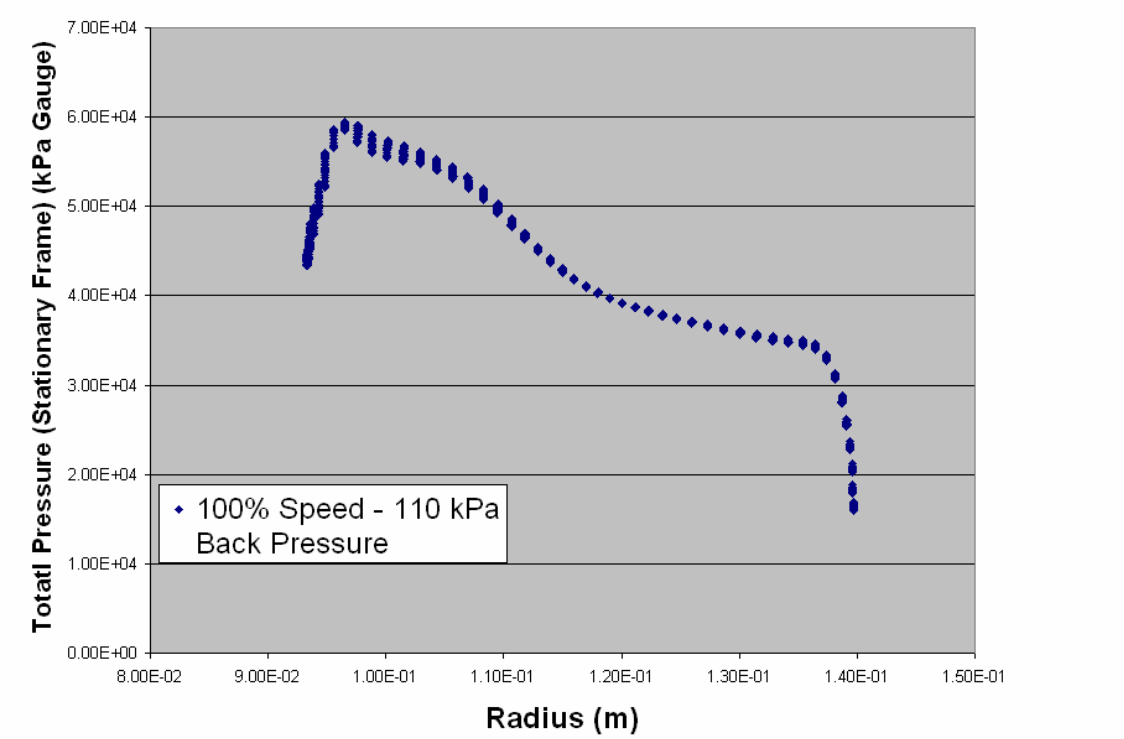
Totatl Pressure (Stationary Frame) (kPa Gauge)
7.00E+04
6.00E+04
5.00E+04
4.00E+04
3.00E+04
2.00E+04
1.00E+04
0.00E+00
8.00E-02
9.00E-02
1.00E-01
1.10E-01
1.20E-01
1.30E-01
1.40E-01
1.50E-01
Radius (m)
100% Speed - 110 kPa Back Pressure

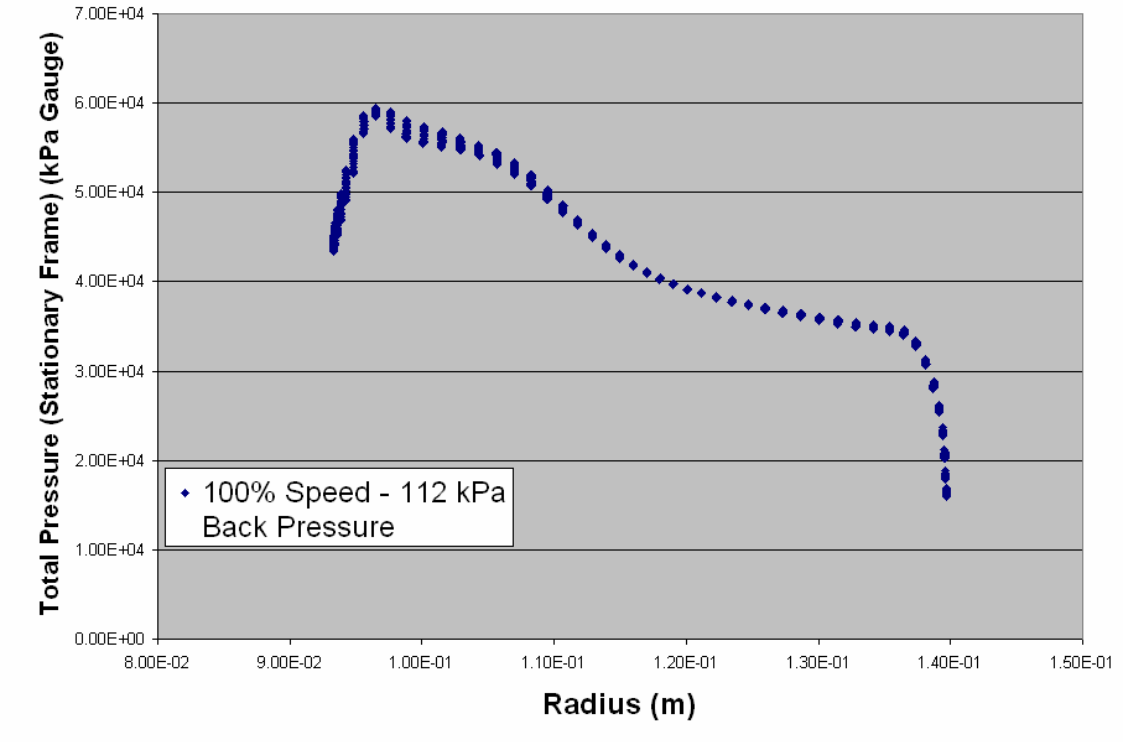
Total Pressure (Stationary Frame) (kPa Gauge)
7.00E+04
6.00E+04
5.00E+04
4.00E+04
3.00E+04
2.00E+04
1.00E+04
0.00E+00
8.00E-02
9.00E-02
1.00E-01
1.10E-01
1.20E-01
1.30E-01
1.40E-01
1.50E-01
Radius (m)
100% Speed - 112 kPa Back Pressure

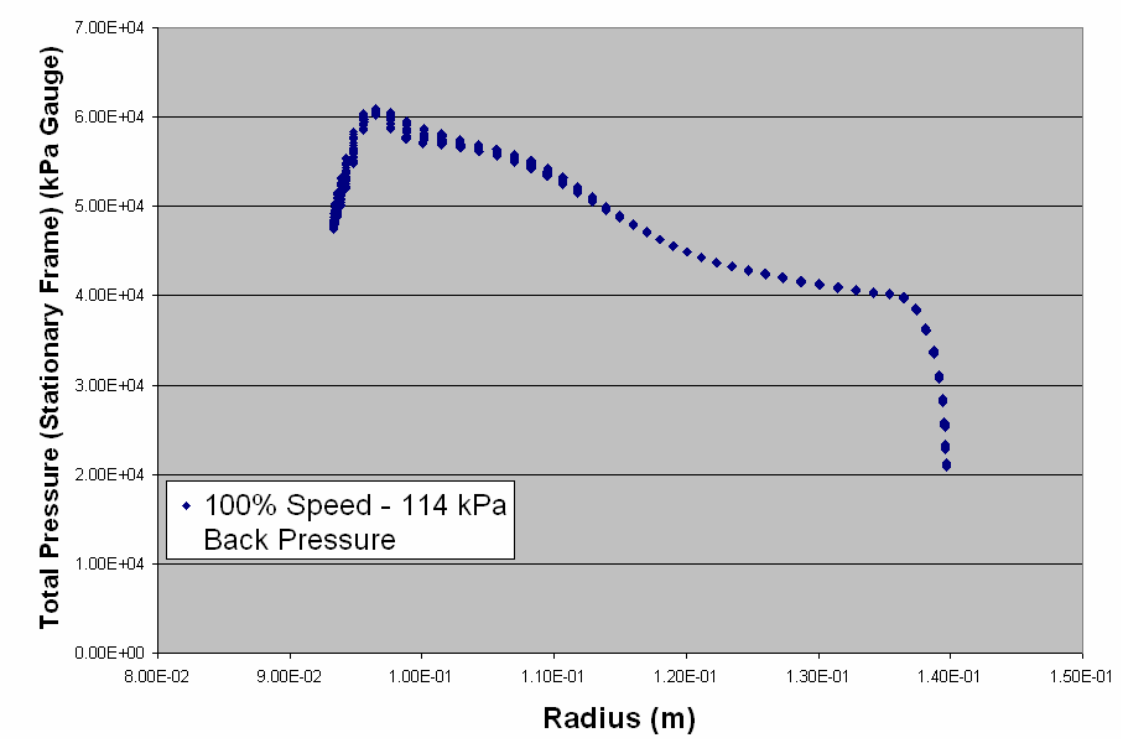
Total Pressure (Stationary Frame) (kPa Gauge)
7.00E+04
6.00E+04
5.00E+04
4.00E+04
3.00E+04
2.00E+04
1.00E+04
0.00E+00
8.00E-02
9.00E-02
1.00E-01
1.10E-01
1.20E-01
1.30E-01
1.40E-01
1.50E-01
Radius (m)
100% Speed - 114 kPa Back Pressure

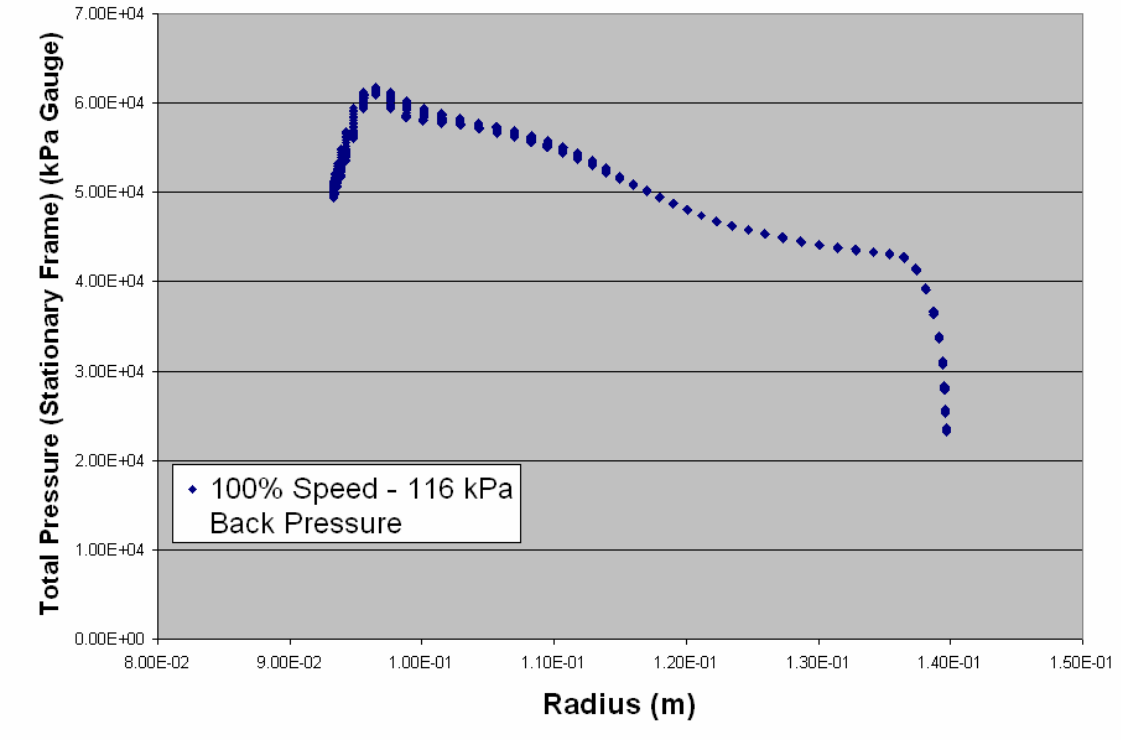
Total Pressure (Stationary Frame) (kPa Gauge)
7.00E+04
6.00E+04
5.00E+04
4.00E+04
3.00E+04
2.00E+04
1.00E+04
0.00E+00
8.00E-02
9.00E-02
1.00E-01
1.10E-01
1.20E-01
1.30E-01
1.40E-01
1.50E-01
Radius (m)
100% Speed - 116 kPa Back Pressure

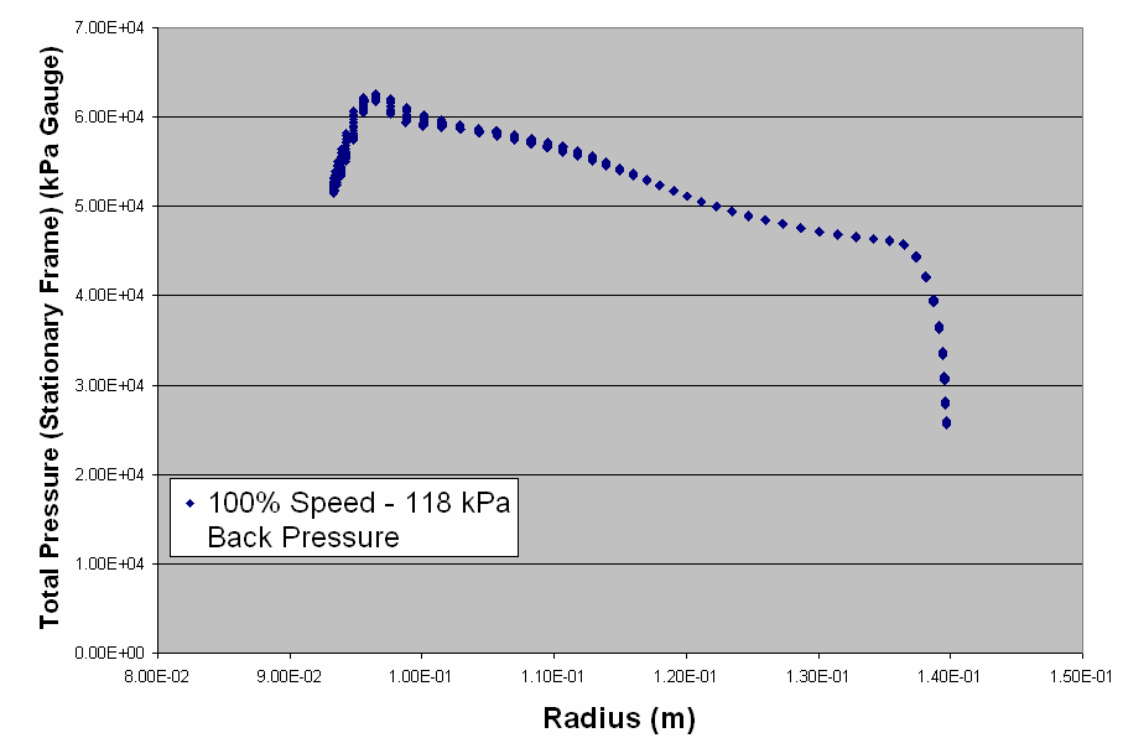
Total Pressure (Stationary Frame) (kPa Gauge)
7.00E+04
6.00E+04
5.00E+04
4.00E+04
3.00E+04
2.00E+04
1.00E+04
0.00E+00
8.00E-02
9.00E-02
1.00E-01
1.10E-01
1.20E-01
1.30E-01
1.40E-01
1.50E-01
Radius (m)
100% Speed - 118 kPa Back Pressure

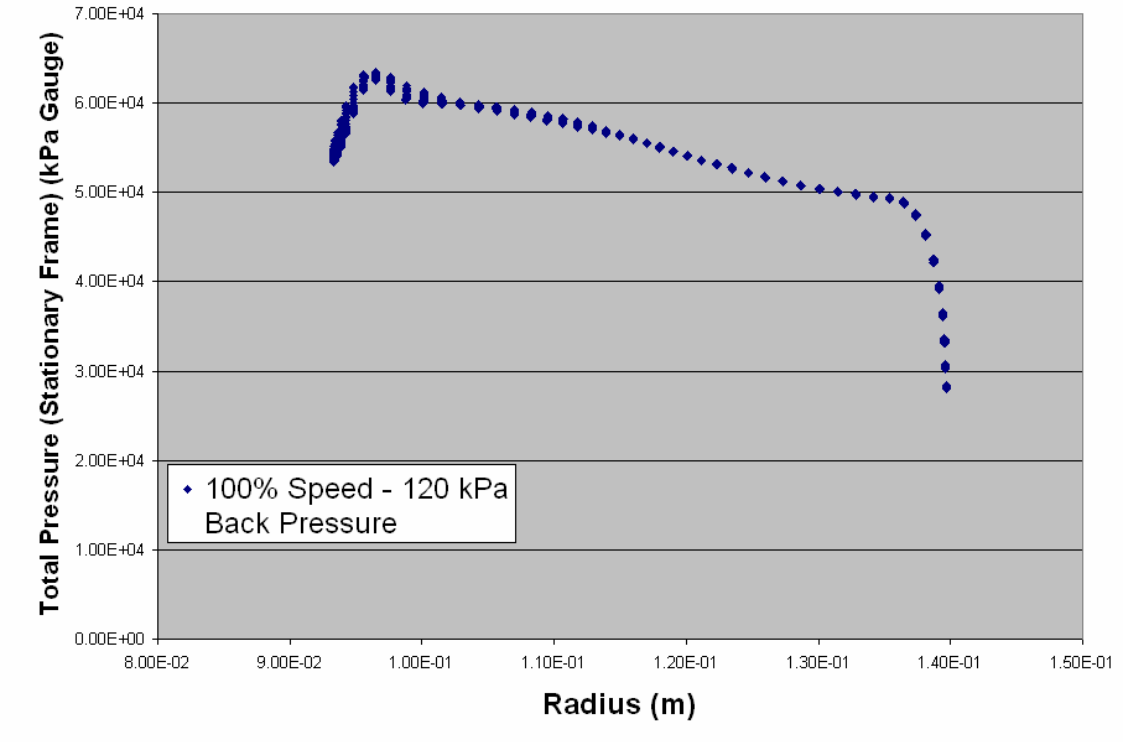
Total Pressure (Stationary Frame) (kPa Gauge)
7.00E+04
6.00E+04
5.00E+04
4.00E+04
3.00E+04
2.00E+04
1.00E+04
0.00E+00
8.00E-02
9.00E-02
1.00E-01
1.10E-01
1.20E-01
1.30E-01
1.40E-01
1.50E-01
Radius (m)
100% Speed - 120 kPa Back Pressure

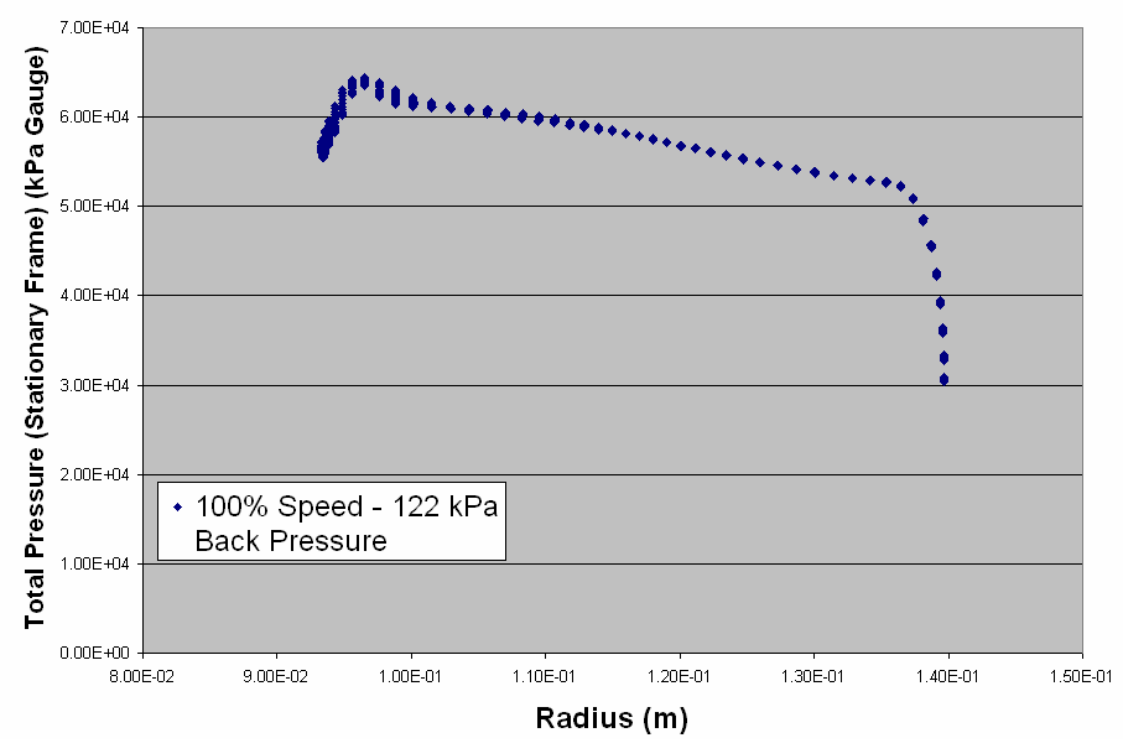
Total Pressure (Stationary Frame) (kPa Gauge)
7.00E+04
6.00E+04
5.00E+04
4.00E+04
3.00E+04
2.00E+04
1.00E+04
0.00E+00
8.00E-02
9.00E-02
1.00E-01
1.10E-01
1.20E-01
1.30E-01
1.40E-01
1.50E-01
Radius (m)
100% Speed - 122 kPa Back Pressure

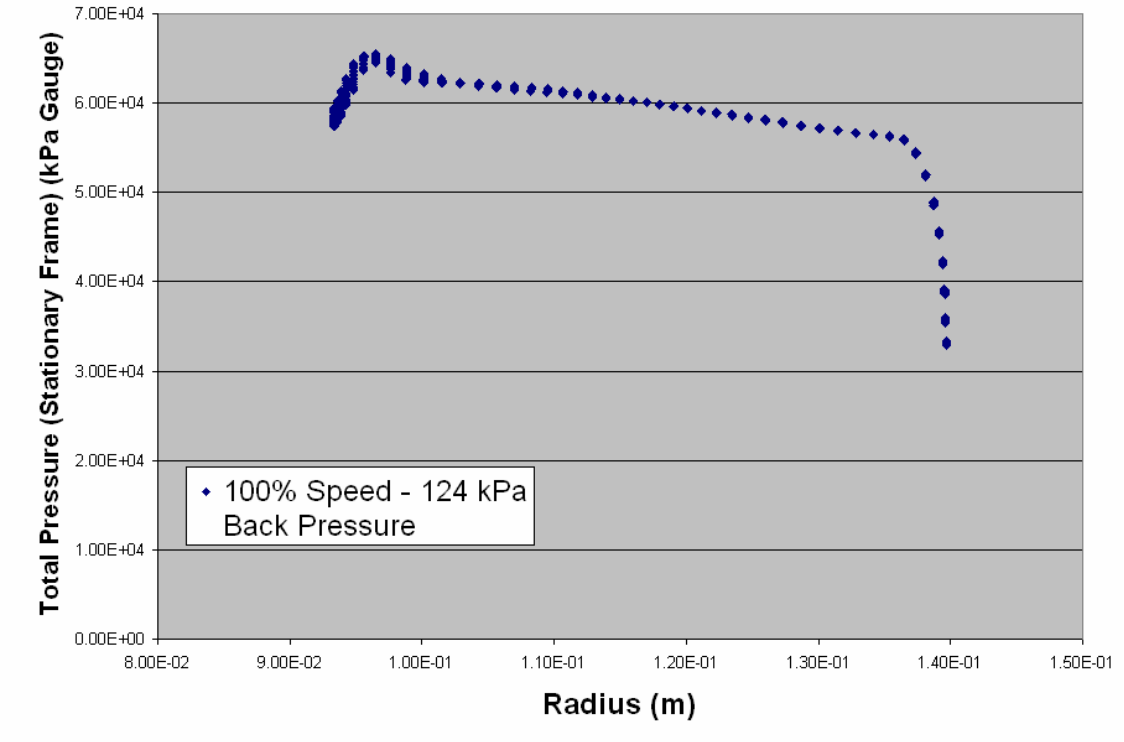
Total Pressure (Stationary Frame) (kPa Gauge)
7.00E+04
6.00E+04
5.00E+04
4.00E+04
3.00E+04
2.00E+04
1.00E+04
0.00E+00
8.00E-02
9.00E-02
1.00E-01
1.10E-01
1.20E-01
1.30E-01
1.40E-01
1.50E-01
Radius (m)
100% Speed - 124 kPa Back Pressure

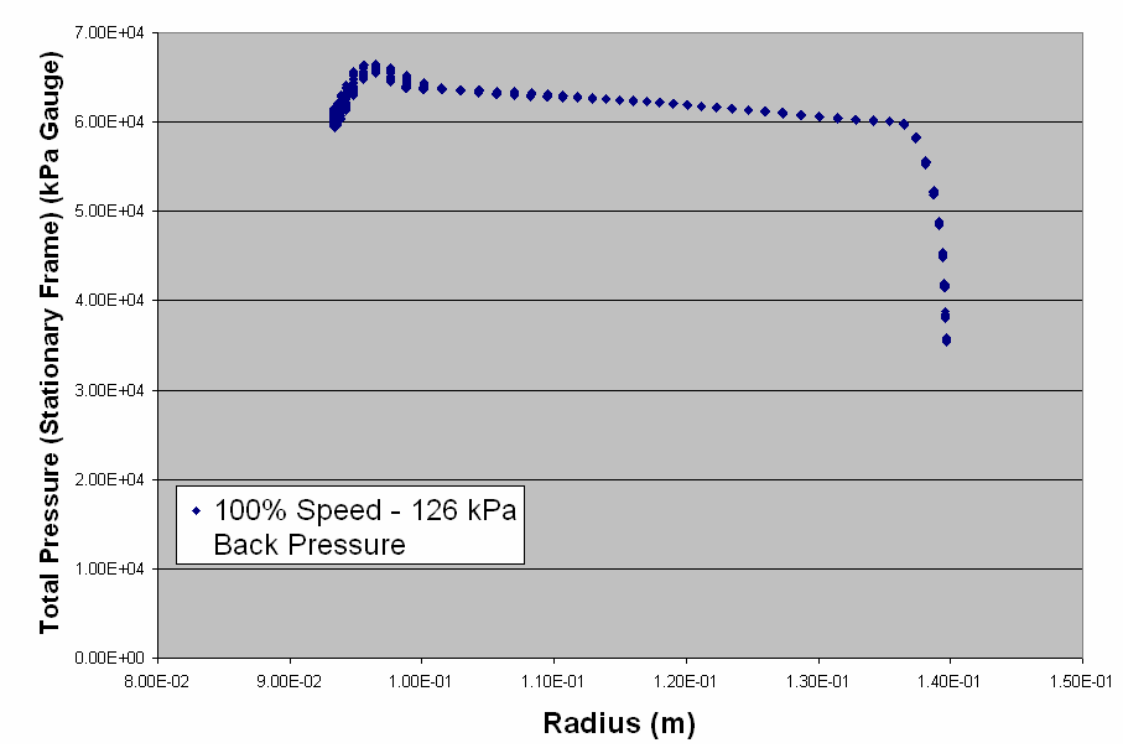
Total Pressure (Stationary Frame) (kPa Gauge)
7.00E+04
6.00E+04
5.00E+04
4.00E+04
3.00E+04
2.00E+04
1.00E+04
0.00E+00
8.00E-02
9.00E-02
1.00E-01
1.10E-01
1.20E-01
1.30E-01
1.40E-01
1.50E-01
Radius (m)
100% Speed - 126 kPa Back Pressure

THIS PAGE INTENTIONALLY LEFT BLANK

APPENDIX C: PROCEDURE FOR DEVELOPING BLADE PASSAGE

1. Geometry
    - Points
        - Insert Point Manually
        - Enter the Coordinates (0,0,0). This will define a reference point
2. File
    - Import Geometry
        - Formatted Point Data.
        - Select files that contain the data points
3. Geometry
    - Curves
        - Curves Through Points. Create all necessary lines for blade, hub, and tip.
4. Geometry
    - Surfaces
        - From Curves. Create all necessary surfaces for blade, hub, tip, inlet, outlet, symmetry side 1, and symmetry side 2.
5. Geometry
    - Curves
        - Project curve onto surface (as needed). Delete old curve.
6. Blocking
    - Create Block
        - Initialize Block 3-D
7. Mesh
    - Global Mesh Size
        - Define Periodicity (make sure check is in box)
        - Rotationally Periodic
        - Axis = 1 0 0
        - Angle = 16.3636
8. Blocking
    - Edit Block
        - Periodic Nodes. Group Nodes together to ensure periodicity.
        - Periodic Nodes will move 16.3636 degrees apart
9. Blocking
    - Associate
        - Edit Associations
            - Associate Edge/Curve. Highlight all edges of the block. Click middle mouse button. Highlight all the outside curves of the passage. Click middle mouse button. Click Apply.

10. Blocking
    Associate
        Edit Associations
            Associate Vertex/Point. Click on a vertex and its corresponding point. The vertex and the periodic vertex will move.
11. Blocking
    Edit Edge
        Edit Edge w/ linear split. Create splits in the block edges so that they map to the corresponding curves

12. Blocking
    Split Block
        Split Block. From a top down view place two splits in the block. One forward of the blade and one aft. Place two additional splits in the blade. One on top and one on the bottom of the blade.
13. Blocking
    Associate
        Edit Associations
            Associate Edge/Curve. Highlight the curves that are the top of the blade. Click the middle mouse button. Highlight the edges that correspond to those curves. Click the middle mouse button. Press Apply.
14. Blocking
    Associate
        Edit Associations
            Associate Vertex/Point. Associate the vertex of the block to the points on the blade where the leading/trailing edge begin/end.
15. Blocking
    Edit Edge
        Edit Edge w/ linear split. Create splits in the blocks edge so that it map's to the curve of the blade.
16. Repeat Steps 13 – 15 for the bottom of the blade.
17. Blocking
    Split Block
        "O"-grid Block
        Ensure the "Around Block" function is checked. Highlight the block in the blade and press delete.
18. Blocking
    Move Vertices
        Move Vertex. This will allow you to change the vertex positions along the edges of the blocks to develop a more even mesh.

19. Mesh
    Surface Mesh Size
        Ensure all the surfaces are activated. Highlight all the surfaces and click the middle mouse button. Change the default data to .01 for the first three fields.
20. Left Side of Screen
    Bottom Window
        Right click on surfaces. Activate Hexa Sizes. Exam the CAD drawing to ensure sizes are appropriate and then deactivate Hexa Sizes.
21. Blocking
    Pre-Mesh Params
        Recalculate Sizes. Ensure the update all button is activated and click apply. This will apply the mesh size to the entire mesh, not just the surface mesh.
22. Left Side of Screen
    Bottom Window
        Click on "plus" sign next to blocks.
        Right click on Pre-Mesh
        Recompute. This will load the premesh. If it is good, then continue. If not, use the Blocking functions to move vertices and associate edges accordingly.
23. Left Side of Screen
    Bottom Window
        Right click on Pre-Mesh and activate "solid". This will produce the solid volume mesh. Ensure that no elements protrude into the blade. If not elements protrude into blade, then deactivate "solid".
24. Blocking
    Pre-Mesh Params
        Edit Edge. Change the number of elements on the edges by highlighting an edge and clicking the middle mouse. In the number of nodes field enter the number desired. Also, change the spacing of the nodes in this area so that more nodes are placed closer to the hub and tip as well as closer to the blade. This is accomplished through the use of exponential spacing and indicating a small spacing size. ENSURE THAT COPY TO PARALLEL EDGES HAS BEEN ACTIVATED!
25. Left Side of Screen
    Bottom Window
        Blocks
            Pre-Mesh. Right click and click on recompute. If the mesh is satisfactory then continue. If not then make the necessary changes.

26. Left Side of Screen
    Bottom Window
        Blocks
            Pre-Mesh. Right click and click on Convert to Unstructured Mesh. This will create the mesh.
27. Output
    Select Solver
        CFX-5. Click Okay.
28. Output
    Write Input
        Click Yes for save current project first.
        Change output file to: BladePassage.cfx5
        Press Done.
29. Open CFX-5 and load this mesh there.

INITIAL DISTRIBUTION LIST

1. Defense Technical Information Center
   Ft. Belvoir, Virginia

2. Dudley Knox Library
   Naval Postgraduate School
   Monterey, California

3. Distinguished Professor and Chairman Anthony Healey
   Department of Mechanical and Aeronautical Engineering
   Naval Postgraduate School
   Monterey, California

4. Professor Raymond Shreeve
   Department of Mechanical and Aeronautical Engineering
   Naval Postgraduate School
   Monterey, California

5. Professor Garth Hobson
   Department of Mechanical and Aeronautical Engineering
   Naval Postgraduate School
   Monterey, California

6. Dr. Anthony Gannon
   Department of Mechanical and Aeronautical Engineering
   Naval Postgraduate School
   Monterey, California

7. Naval Air Warfare Center
   Propulsion and Power Engineering
   ATTN: Mark Klein
   Patuxent River, Maryland

8. ENS Nikolaus Bochette
   Monterey, California